MXenes and their derivatives as nitrogen reduction reaction catalysts: Recent progress and perspectives

Tahta Amrillah[1], Angga Hermawan[2,*], Vani Novita Alviani[3], Zhi Wei Seh[4], Shu Yin[5,*]

[1]*Department of Nanotechnology, Faculty of Advanced Technology and Multidiscipline, Universitas Airlangga, Surabaya 60115, Indonesia*

[2]*Faculty of Textile Science and Technology, Shinshu University, 3-15-1 Tokida, Ueda City, Nagano 386-8567, Japan*

[3]*Graduate School of Environmental Studies, Tohoku University, Sendai 9808579, Japan*

[4]*Institute of Materials Research and Engineering, Agency for Science, Technology and Research (A*STAR), 138634, Singapore*

[5]*Institute of Multidisciplinary Research for Advanced Material (IMRAM), Tohoku University 2-1-1 Katahira, Aoba-ku, Sendai, Miyagi 980-8577, Japan*

Contact: angga@shinshu-u.ac.jp and yin.shu.b5@tohoku.ac.jp

Abstract:

MXenes have become one of the most actively studied emerging materials. They hold great promise as efficient catalysts for chemical conversion and environmental purification due to their unique layered structure, high specific surface area, abundant active sites, and excellent chemical stability. Recent breakthroughs have demonstrated MXenes and their derivatives in adsorbing, activating, and converting nitrogen (N_2) to ammonia (NH_3) *via* electrocatalytic and photocatalytic nitrogen reduction reaction (NRR). The NRR is a green and environmentally friendly NH_3 synthesis utilizing N_2 and water molecules under mild conditions, unlike the current-day Haber-Bosch technology that directly uses fossil fuel with intensive energy processes. However, the NH_3 yield and efficiency of NRR using MXene-based catalysts remain too low to meet practical applications. Therefore, a fundamental understanding of NRR mechanisms and their significant challenges should be addressed for future development. In this review, a theoretical investigation of the promising properties of MXenes as NRR catalysts is summarized. The recent development of MXenes and their derivatives in NRR and their enhancement strategies are discussed. The synthesis protocols to obtain tunable morphology, nanocomposites-based, and derivatives of MXenes are also presented. Eventually, we provide new perspectives to direct future research in realizing clean and sustainable NH_3 production.

1. Introduction

Nitrogen (N_2) is the most abundant element in the Earth's atmosphere as well as an essential natural feedstock for the production of intermediate chemicals, notably ammonia (NH_3) and hydrazine (N_2H_4) [1,2]. NH_3 alone is a primary component of fertilizer that feeds the global food supply [2,3]. It is also an imperative nitrogen source in manufacturing explosives, resin, and pharmaceuticals. In addition, N_2H_4 can be derived from the oxidative coupling process of NH_3. Chemically converting or "fixing" N_2 is unfortunately exhausting due to its chemical inertness [3,4]. In a conventional and century-old industrial making known as the Haber-Bosch (HB) process, the synthesis of NH_3 requires massive energy to dissociate the triple bond ($N\equiv N$) of N_2 [4–6]. The HB process generally involves N_2 and H_2 as feed gases with high-temperature (above 350 ^oC) and pressure (above 150 atm) using iron (Fe)− or ruthenium (Ru)−based catalysts [6,7]. Therefore, many researchers and scientists have been devoting effort to developing alternative sustainable technologies for NH_3 synthesis.

Adopting a natural process of N_2 fixation using nitrogenase enzyme in azotobacterial, an artificial NH_3 synthesis through electrocatalytic and photocatalytic nitrogen reduction reaction (NRR) has gained significant attention over the last decades [8–11]. This is mainly because the synthesis process is possibly undertaken under mild conditions (such as room temperature and atmospheric pressure) with only N_2 and water as the fuel sources [9,10,12–14]. It excludes a fossil fuel feedstock, so that further eliminates the by-product CO_2. The NRR pathway during electrochemical and photochemical processes proceeds by adding protons and electrons [15]. The protons are taken from H_2O molecules, and electrons come from solar energy (photocatalytic) and other renewable electricity sources (electrocatalytic) [15,16]. It is believed that the overall features of these processes can afford to tackle the environmental and energy concerns in present-day NH_3 production [14]. Unfortunately, the NH_3 yield and selectivity *via* electrocatalytic and photocatalytic NRR routes are relatively low [9,17]. To date, finding an alternative, efficient, and non-precious metal catalyst able to compete with noble metal catalysts (*e.g.*, Au, Pt, Pd, Ru, Ir, and Rh) remains a significant challenge to address the general requirement of high NH_3 yield and excellent selectivity for NRR [18–20]. To this end, two-dimensional (2D) catalysts with large specific surface areas and great exposed active sites for N_2 adsorption and activations are expected to perform well in photochemical and electrochemical N_2 fixation to NH_3 [21].

In recent years, a new and large family of 2D layered materials founded in 2011, named MXenes, emerged as one of the most advanced materials [22]. It is evident from their substantial applications in various emerging fields, including energy storage systems [23–26], sensors [27–29], catalysts [30–36], environmental remediation [37–39], biomedicals [40–42], optoelectronics [43–45], electromagnetic shielding [46], and even in additive manufacturing [47]. The exceptional properties of MXenes are obtained from their diverse chemical compositions, elemental abundance in the Earth, large surface dimensional ratio, tunable surface functionalities, high electrical conductivity, and exceptional strength and stability [48,49]. The general composition of MXenes is $M_{n+1}X_nT_x$, where M represents a transition metal, X can be either carbon and/or nitrogen, T represents a surface termination group (–O, –F, –OH), while n denotes 1 to 4. MXenes are obtained by HF selective etching from their $M_{n+1}AX_n$ phase precursors, where A is group III, usually aluminum (Al) [22,24,50]. In the NRR application, MXenes are expected to be a potential catalyst for electrocatalytic and photocatalytic N_2 fixation based on the previously highlighted properties, despite the preliminary work that started not long ago. As shown in **Fig. 1**, in 2016, Azofra *et al.* [51] first reported a promising prospect of MXenes as novel catalysts for N_2 reduction to NH_3 based on their density functional theory (DFT) investigations owing to the large spontaneous Gibbs free binding energy for N_2 capture and activation. With a similar approach, Shao *et al.* [52] reported the efficient N_2 fixation to NH_3 on binary (M_2C) MXenes. Following these pioneering computational studies, in the same year, Zhao *et al.* [53] performed the first experimental work on 2D $Ti_3C_2T_x$ (T= F, OH) MXene for N_2 electroreduction to yield NH_3 of 20.4 $\mu g\ h^{-1}\ mg_{cat.}^{-1}$. The design and preparation of MXenes derivatives for N_2 photofixation were revealed by Liu *et al.* [54] to achieve an NH_3 yield rate of 250.6 $\mu mol\ g_{cat.}^{-1}\ h^{-1}$ under visible light irradiation. Since then, many researchers have devoted efforts to optimize the performance of MXenes and MXene derivatives-based catalysts for efficient NRR, such as introducing single-atom and molecular catalysts, surface engineering, morphological modification, tuning chemical composition, etc.
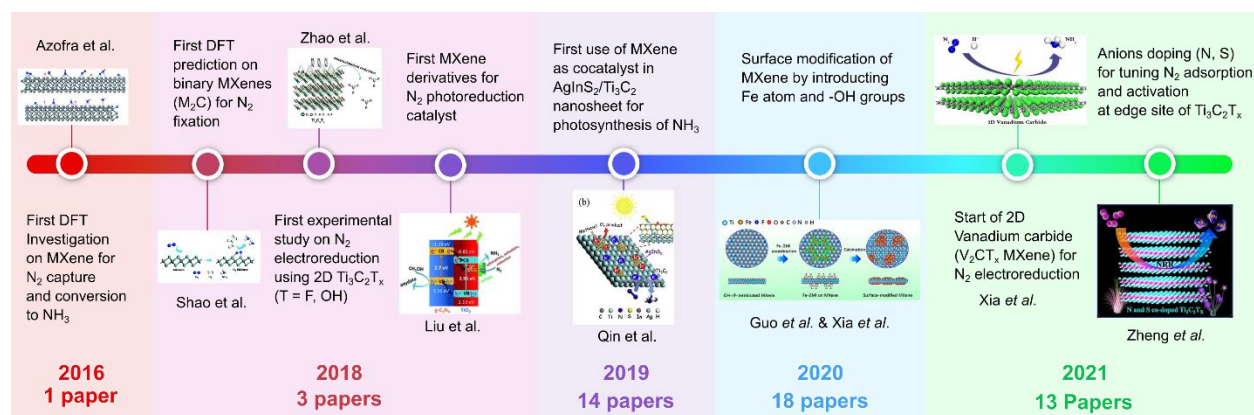
Fig. 1 Historical development of MXenes as electrocatalyst and photocatalysts for N_2 fixation to NH_3.

There are some reviews published elsewhere highlighting the progress of MXenes and MXene-derivatives applications, such as for photocatalysts [31,55,56], electrocatalysts [21,57,58], and energy storage and conversion [24,50,59,60]. More specifically, Sun *et al.* [61] and Leong et al. [62] recently provided insightful reviews on MXenes-based electrochemical NRR catalysts. Nevertheless, both did not summarize the recent advances in applying MXenes or their derivatives as co-catalysts in photochemical N_2 reduction, nor predicting the NRR pathway catalysts surface with significant computational methods, nor screening the potential and efficient catalysts. Since the research progress of MXenes and MXenes derivatives is accelerating rapidly, a comprehensive summary on the latest development of MXenes and MXenes-derived catalysts for NRR applications is a requisite to provide a helicopter view of how this research field should be directed. Therefore, this review aims to present a timely and comprehensive discussion, starting from discovering MXenes as promising materials for N_2 capture and fixation, followed by an in-depth discussion of the theoretical screening using computational simulations. We have also summarized *state-of-the-art* developments on the use of MXenes and MXenes derivatives as catalysts in NRR and their preparation methods. Finally, the existing challenges and perspectives for future efforts to optimize MXenes-based catalysts for NRR are provided. We expect this review will stimulate meaningful research and essential developments on these emerging MXenes catalysts.

2. Mechanism of the electrocatalytic and photocatalytic nitrogen reduction reaction

In pursuance of improving the catalytic activity and efficiency and realizing various strategies over the electrochemical NRR, it is important to comprehend the process of N_2 reduction

into NH_3. Due to the strong non-polar N_2 triple bond, the electrochemical NRR is quite challenging in practice and engages in heterogeneous reactions with three elementary steps of adsorption and activation, hydrogenation, and desorption. The N_2 adsorption and activation is the first important step in the electrochemical NRR related to the electronic donation/acceptation process to active sites on the electrocatalysts' surface, thus weakening the $N{\equiv}N$ bond. Hydrogenation involves a series of steps of breaking triple bonds and the formation of the N—H bonds. The desorption step is associated with the desorption of NH_3 molecules.

The electrochemical mechanisms of N_2 reduction into NH_3 are generally classified into dissociative and associative mechanisms according to different hydrogenation sequences and the breaking of the N_2 triple bond [63–66], see **Fig. 2**. In the dissociative pathway, the $N{\equiv}N$ bond is broken in the process of adsorption, which then individual N atoms are separated by a distinct distance. The formation of NH_3 molecules from each N atom occurs independently in the hydrogenation step (**Fig. 2**). The high activation energy in this pathway is requisite to solve the high-kinetic energy barrier in the direct breaking process of the $N{\equiv}N$ bond. Therefore, the dissociative mechanism prevailing in the current Haber-Bosch process is related to the high temperatures and pressures required for the $N{\equiv}N$ bond's cleavage.

For the associative pathway, the $N{\equiv}N$ bond stays intact after the adsorption step but later breaks at a particular step in the hydrogenation process. The associative route has more complicated steps than the dissociative pathway and can be divided into three possible pathways: distal, alternating, and enzymatic pathways. In the distal pathway, after N_2 adsorption, hydrogenation occurs at one of the two N atoms away from the catalytic surface to release the first NH_3, and continuous hydrogenation of another N atom will produce another NH_3 molecule (**Fig. 2 (a)**). Unlike the consecutive hydrogenation of the distal pathway, the hydrogenation step in the alternating pathway takes place alternatively on the two N atoms. At first, one of the N atoms in the N_2 molecule adsorbs on the electrocatalyst surface. After breaking the $N{\equiv}N$ bond, one of the N atoms releases the first NH_3, and the N—N bond breaks. The remained NH_2 accepts one more proton to form the second NH_3 molecule (**Fig. 2 (a)**). Meanwhile, the enzymatic pathway indicates a distinctive feature than the alternating and distal routes. It presents N_2 adsorption laterally on the catalyst's surface at the first step in the enzymatic pathway (**Fig. 2 (a)**). The following hydrogenation steps are identical to those in the alternating pathway. The distal, alternating, and

enzymatic pathways dominate electrochemical NRR because the N≡N bond's cleavage is unnecessary, making reactions involved in relatively mild conditions, further reducing the energy input. For that analogous reason, associative pathways might be considered the most favorable mechanism for electrochemical NRR on the MXenes catalysts.

The catalytic NRR mechanism over photocatalysts involves several steps before the reduction of N_2 and the generation of NH_3 molecules [17]. As shown in **Fig. 2 (b)**, at the first step, the photogenerated electrons and holes will occupy the conduction and valence bands during the light illumination, respectively. In a subsequent step, some portions of the photogenerated electron-holes pair will recombine, and some of them will take part in the reduction and oxidation reaction on the photocatalysts' surface [67]. The photogenerated holes will oxidize the H_2O molecules into O_2 molecules, while the photogenerated electrons will reduce N_2 into NH_3 molecules [68]. The light intensity and wavelength are important factors for drifting these reactions. If the light intensity is too low, only a few photogenerated electron-holes pairs may involve in the redox reaction, while if it is too high, the photocatalyst may not be stable for such a long period. The optical wavelength should exceed the photocatalysts' bandgap energy to ensure the photogenerated electrons gain enough energy to jump to the conduction band.
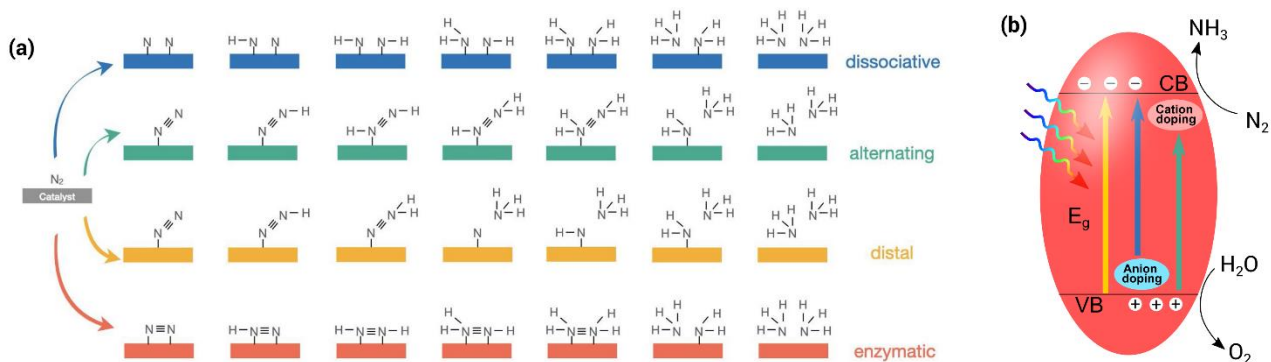

Fig. 2 (a) Various pathways of electrocatalytic and (b) photocatalytic nitrogen reduction reaction (NRR) mechanisms. (a) is reproduced from [62]. Copyright 2021, Elsevier B.V.

3. Discovery and exploration of MXenes as N_2 reduction catalyst using computational simulation

Thanks to modern experimental and computational resources, investigations, and modifications on MXenes, electrocatalytic N_2 fixation is increasingly expanded [61]. MXenes, due mainly to their intrinsic stable chemical bonds of N_2, a mass portion of the energy is necessary to prevail over the kinetic limitation of NH_3 production [69]. Therefore, a proper advanced modification and well-designed MXenes-based catalyst will provide an avenue to decrease energy reaction, and the NRR can proceed under relatively ambient conditions. The recent theoretical approach of MXenes has been extensively addressed to obtain proper combination elements to form MXenes for N_2 catalyst, especially DFT calculation [70]. DFT calculation is a common method used to study the feasibility of MXenes as N_2 catalysts. Various DFT calculation approaches have been developed to obtain and predict the properties and efficiency of MXenes-based catalysts. In a pioneering study, the middle Ti at the edge sites appeared as an active site for the NRR [71]. The N_2 dissociation also developed easily on the (0001) surface, where the top site above the metal ions on the MXene nanosheets surface was indicated as the active site for end-on adsorption of N_2 [71]. Ti_3C_2 with a 2D- or nanosheet structure was useful for N_2 fixation, having the activity related to edge planes as illustrated in **Fig. 3 (a) and (b)** [71]. In DFT, we can also use a scaling relationship and Bader charge analysis to deliver an in-depth understanding of the NRR process in single-atom catalysts anchored on 2D MXenes [72]. In fact, even in traditional Ti_3C_2 MXenes, their catalysts' feasibility has been calculated using the DFT, resulting in excellent N_2 adsorption (–1.34 eV) [73]. Also, according to the first DFT calculations of MXene as NRR catalysts, we could determine that V_3C_2 and Nb_3C_2 showed the most promising candidates of all M_3C_2 carbides studied (M = Ti, Zr, Hf, V, Nb, Ta, Cr, and Mo) having high over-potentials of 0.64 eV and 0.9 eV, individually [61]. Several works using DFT calculations have been used to analyze the feasibility of any MXenes, including the Mo_2TiC_2-MXene that was strongly predicted suitable for electrocatalyst of NH_3 synthesis since N_2 was very easy to occupy the Mo active site and thus induced higher Faradaic efficiency (FE) [69]. MXene with M_2X structures (M = Mo, W, Ta, or Ti; X=C or N) also have been studied using DFT [52], and it turned out that W_2C and Mo_2C monolayers for N_2 fixation had higher efficiencies amongst other M_2X-based MXenes because nearly all of the steps provided an exothermic reaction and relatively low reaction energy. The theoretical approach of MXenes for photocatalyst application has been conducted likewise. Using DFT calculations, it was reported

that the Sc_2CF_2, $Sc_2C(OH)_2$, Sc_2CO_2, Ti_2CO_2, Zr_2CO_2, Hf_2CO_2, and Y_2CF_2 were predicted to exhibit semiconductor properties, including bandgaps between 0.24 to 1.8 eV, which found suitable for photocatalytic applications [74,75]. By computational approach, it was then predicted that surface termination of MXenes strongly influenced photocatalytic performance. A finding was that Ti_3C_2 with –O terminations had relatively low Gibbs free energy and excellent hydrogen evolution reaction (HER) activity compared to –F termination [31].
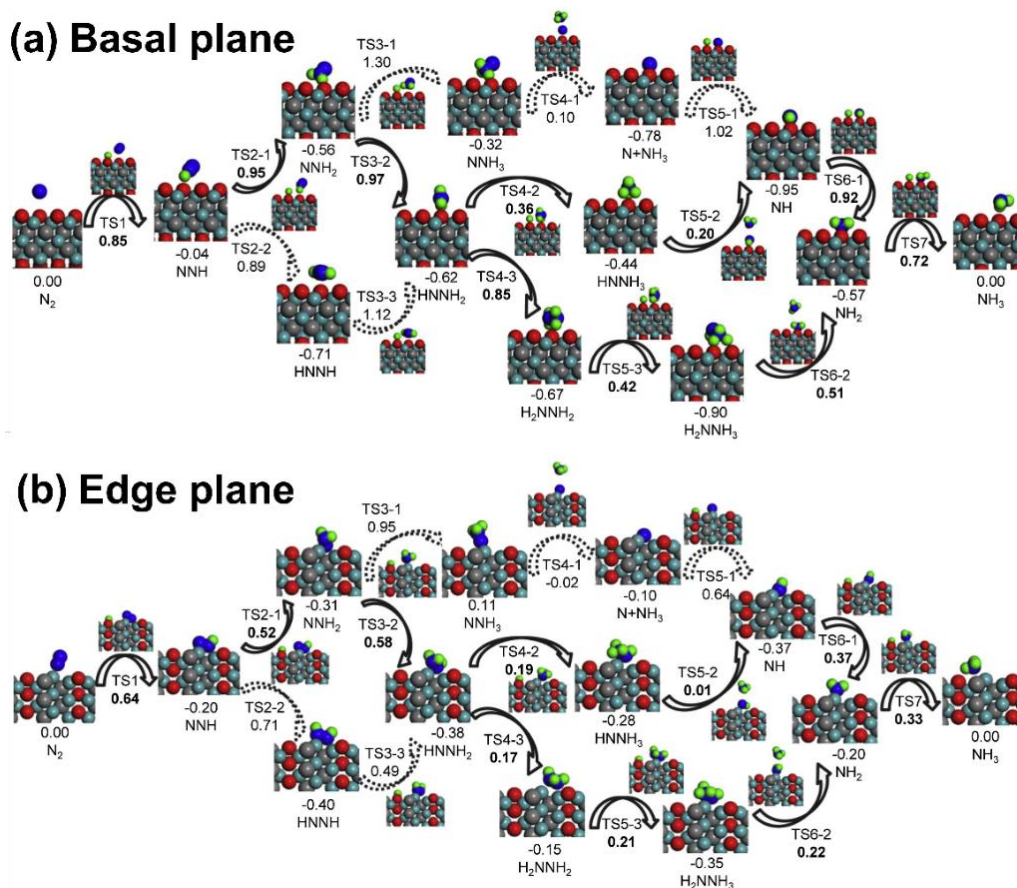

Fig. 3 Comparison of the N_2 reduction reaction pathways on: (a) basal plane and (b) edge plane of $Ti_3C_2T_x$ MXene. Reproduced with permission from [73]. Copyright 2018 Elsevier.

DFT calculation has been conducted not only for the basic structures of MXenes but also for incorporating other elements into the structures of MXenes for N_2 catalysts. For instance, Kong *et al.* [76] have conducted a comprehensive DFT study of 26 transition metal elements supported on Nb_2CN_2 MXenes for its application to electrochemical NRR. Using the DFT study, it was determined that the single-atom catalyst could strongly merge with Nb_2CN_2 *via* transition metal –

3N configuration leading to its low overpotential of 0.51 V in a distal mechanism. It was also predicted using DFT that the incorporation of transition metal elements in Nb_2CN_2 could induce high selectivity to NRR by hindering the hydrogen adsorption and the HER. In the case of incorporation of single-atom catalyst (SACs) on MXenes, the DFT calculation of Ti_3C_2/Au nanocomposite showed high energy adsorbed by N_2 at the site of Au with O atom anchoring could weaken the N triple bonds and reduce the activation energy barrier, which was responsible for their sophisticated average NH_3 yield of 30.06 μgh^{-1} $mg_{cat.}^{-1}$ and a high FE of 18.34%, accordingly [77]. The NRR mechanism proceeded *via* an alternating pathway with the potential limiting step of N_2 fixation was the transformation of the NH_2NH_2* group. Meanwhile, Huang *et al.* [78] discovered a different phenomenon in Ru and Mo anchored Mo_2CO_2 and Ti_2CO_2 where the NRR *via* distal pathway was preferable with a limiting potential of –0.46 V for Ru@Mo_2CO_2.

Additionally, DFT calculation suggested that in TiO_2/$Ti_3C_2T_x$ nanocomposite, the Ti−edge atoms and oxygen vacancies provided in TiO_2 with (101) facet served as active sites to activate and polarize the N molecules. NRR in this TiO_2/$Ti_3C_2T_x$ nanocomposite proceeded through a distal mechanism where the composite exhibited a low energy barrier for N_2 fixation to NH_3, shown in **Fig. 4 (a) and (b)** [79]. As for photocatalyst, Qin *et al.* used DFT calculation to understand the NRR mechanism of $AgInS_2$/Ti_3C_2 composites [80]. The result showed a promiseful prospect in which the optimized adsorption configurations were chemisorbed on a Ti – Ti tripolymer center through an analogous dinuclear end-on coordinated mode. In this configuration, one N atom was incorporated with Ti – Ti tripolymer, and the rest with Ti – Ti dimers. Because of this configuration, large adsorption energy of about −5.20 eV was obtained; thus, the N_2 activation could be spontaneously achieved once chemically adsorbed on MXene nanosheets.
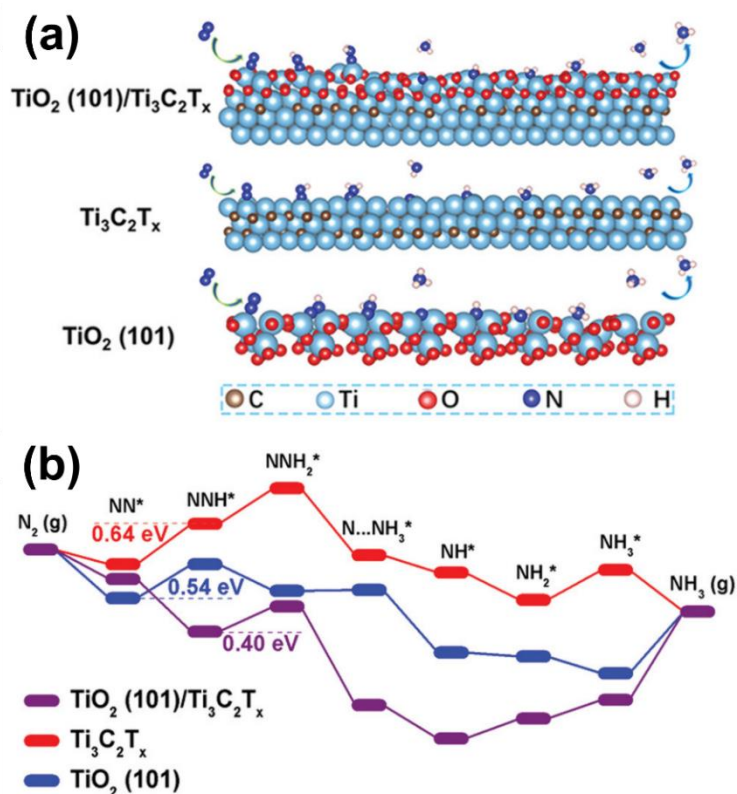
Fig. 4 (a) The optimized structures of the TiO_2 (101)/$Ti_3C_2T_x$, $Ti_3C_2T_x$, TiO_2 (101) surfaces for the NRR through distal mechanisms. (b) Free energy scheme for the NRR on the TiO_2 (101)/$Ti_3C_2T_x$, $Ti_3C_2T_x$, and TiO_2 (101), respectively. Reprinted from [79] with permission. Copyright 2019 Wiley-VCH Verlag GmbH & Co.

4. MXenes and MXenes derivatives catalyst

MXenes are promising catalyst candidates of N_2 capture and reduction, as their performances have been heretofore predicted [6–8]. Many experimental works extend the meaningful and substantial evidence that MXenes can perform competitively with the benchmark of Pt, Co, or Pd−based catalysts in reducing N_2 to NH_3. Besides, one most prominent advantage of MXene as a catalyst is that most chemicals incorporated there are earth-abundant, suggesting that catalyst cost can be significantly reduced without damaging the performance. In NH_3 electrosynthesis, Ti_3C_2/FeOOH exhibited high FE up to 5.78% at an ultralow potential, closer to that of Pt metal [71]. $Ti_3C_2T_x$ nanosheets by intercalation with dimethylsulfoxide (DMSO) also possessed excellent catalytic activity for NRR, having an NH_3 yield of 20.4 µg h^{-1} mg$_{cat.}^{-1}$ with an

FE of 9.3% in acid buffer [81]. Many types of MXenes could be potentially used for the catalyst of the electrochemical NRR, *e.g.*, V_3C_2 and Nb_3C_2, owing to maximum overpotentials of the respective 0.64 and 0.90 eV, and other various MXenes nanocomposites also reported [61]. Various modifications and development of MXenes through advanced synthesis and proper material combinations were conducted to increase the feasibility of MXenes for N_2 catalyst applications.

4.1 MXenes catalyst for electrocatalytic N_2 reduction

In possession of remarkably spontaneous Gibbs free binding energies for N_2 chemisorption, MXenes are able to perform as a catalyst for N_2 capture and reduction [51]. So far, electrocatalytic N_2 reduction has been performed on various types of pristine MXenes, such as $Ti_3C_2T_x$, Mo_2TiC_2, V_2CT_x, and Nb_2CN_2. On the 2D $Ti_3C_2T_x$ MXene nanosheets, the NH_3 yield rate and FE of 20.4 µg h^{-1} $mg_{cat.}^{-1}$ and 9.3% at −0.4 V *vs.* reversible hydrogen electrode (RHE), respectively, could be achieved [81]. It was noteworthy to mention that $Ti_3C_2T_x$ MXene possessed high electrochemical and structural stability against the acidic environment. Conforming to the DFT calculations, N_2 chemisorption on $Ti_3C_2T_x$ could interfere with the bonds of N_2 and thus could facilitate converting N_2 into NH_3. In other cases, V_2CT_x exhibited electrocatalyst ability owing to NH_3 yield rate of 12.6 µg h^{-1} $mg^{-1}_{cat.}$ and an FE of 4% at –0.7 V in 0.1 M Na_2SO_4 environment and electrocatalytic NRR underwent a distal pathway, while Cr sites in Cr_3C_2 MXene were more favorable for enzymatic NRR route as shown in **Fig. 5 (a) and (b)** [82,83]. Whereas, according to DFT on Mo_2TiC_2 MXenes, Mo_2TiC_2 presented both valid N_2−philicity and high catalytic activity for electrocatalytic NH_3 production *via* a dissociation mechanism with a relatively low overpotential of 0.26 V, and the competing HER was simultaneously suppressed [69]. There is still no general agreement to conclude which N_2 reduction mechanism is pursued at this stage since reaction pathways will differ in various MXenes.
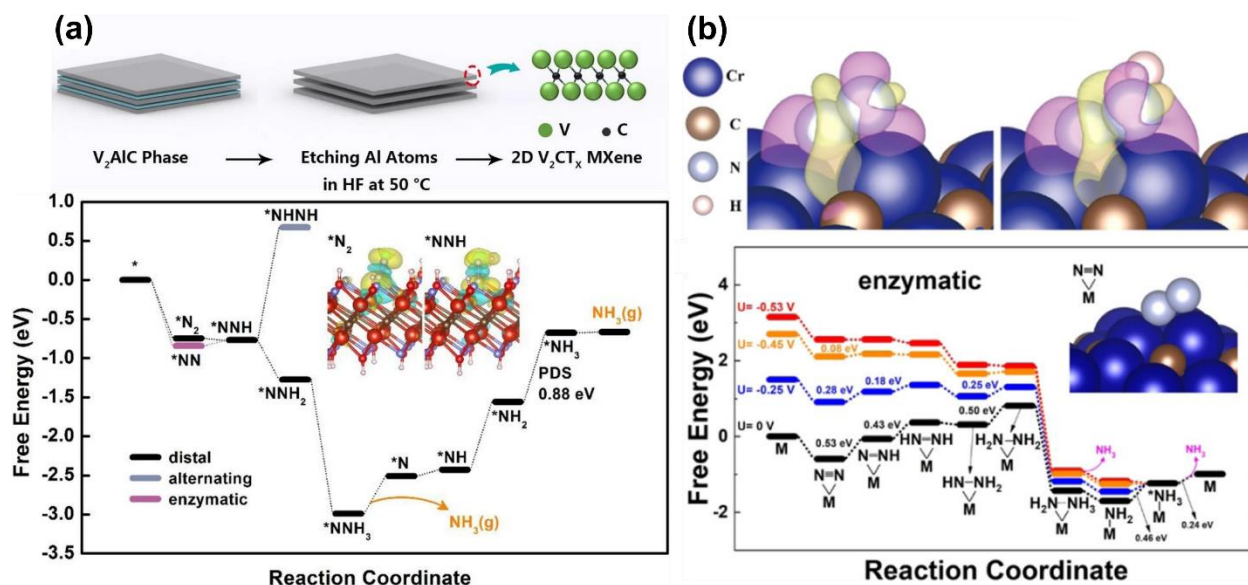
Fig. 5 (a) V_2CT_x synthesis and free energy diagram of N_2 reduction pathway. Adapted from [82] with permission. Copyright 2021 Springer Nature. (b) Free energy diagram of N_2 reduction pathway on Cr_3C_2. Reprinted with permission from [83]. Copyright 2019 American Chemical Society.

MXenes are typically obtained in 2D layered structures, and not impossible to modify their morphology into various shapes and dimensions. Importantly, morphology is one of the governing factors in NRR. Wei *et al.* [84] discovered a significant enhancement in the NRR ability of Ti_3C_2 when it was transformed into a 3D-type nanostructure (nanoribbons) as the formation of exposed Ti – OH sites. Moreover, 3D Ti_3C_2−MXene exhibited a low overpotential of 168 mV at a current density of 10 mA/cm^2 in a 1 M KOH solution. The enhancement of electrocatalytic activity could be related to the hierarchical 3D architecture of the catalysts, enabling them to enhance their active surface area, thus promoting higher charge transfer kinetics and increasing their mass diffusion rate [85]. Not only in 2D or 3D forms, but quantum-dot (0D) forms of MXenes also could be potential to obtain high performance of NRR. It was reported that the hydroxyl-rich $Ti_3C_2T_x$ MXene−derived quantum dots (Ti_3C_2OH QDs) with abundant active sites allowed the development of efficient NRR electrocatalysts. This material offered an NH_3 yield and FE of about 62.94 µg h^{-1} $mg_{cat.}^{-1}$ and 13.30% at −0.50 V [86]. Furthermore, we find that these quantum dot forms of MXenes could be combined with various 2D and 3D materials to realize more enhanced catalyst performance.

The surface of MXenes is of pivotal importance for their application in NRR. Instead of various modifications and development of their surface, maintaining the surface clean from namely contaminants is also essential since contamination could reduce the accessible surface area of MXenes for the NRR process [87]. Several attempts could be used to avoid contamination on the surface of MXenes, for instance, by improving the hydrophilic surface of MXenes. In general, controlling the surface angle during the exfoliation of 2D materials could also change the hydrophilic surface of 2D materials. In any case, improving the hydrophilic surface of 2D could also protect their surface from the contamination originated by airborne organic molecules [87]. In fact, a fabrication process of MXenes is essential to avoid contamination on the surface. Previous reports also indicated that vacuum or inert gas annealing of 2D materials at elevated temperatures being a common way of gaining a pristine surface and interface with the lowest contaminations [88,89]. Strategies to clean the surfaces from unnecessary contamination are vital to obtaining optimal properties of MXenes. Generally, there have been several techniques conducted to clean the surface of 2D materials from surface contaminants and impurities, e.g., by using thermal annealing/desorption, electrical current annealing, washing with some liquid solution; water, acids, bases, ethanol, using plasma treatment, and etching of metals [90].

There have been numerous efforts to enhance the electrochemical activity of pristine MXenes, primarily to modify the surface and structural configurations. Boosting electrosynthesis of NH_3 using MXenes could be realized *via* surface-engineering of MXenes itself, where the N_2 chemisorption took place [91]. As reported previously, Ti_3C_2−MXenes with the increased surface hydroxyl moieties showed enhanced production of NH_3. With the hydroxyl-terminated surface, an NH_3 yield rate and FE at −0.2 V *vs.* RHE at 20 °C were obtained at about 1.71 µg h^{-1} cm^{-2} and 7.01%, respectively [92]. Further optimization by increasing reaction temperature up to 60 °C was effective in producing a yield of NH_3 at 12.46 µg h^{-1} cm^{-2} and an FE of 9.03% at −0.2 V *vs.* RHE. The surface hydroxyl modification of MXenes, revealed by DFT, could effectively facilitate the electron transfer, surface adsorption, and activation of N_2 [92]. It is, however, remaining uncertain if an F−terminated surface can improve MXene-based catalyst performance. In fact, the binding of M–A parts in MXenes is too strong to break, and the formation of a typical layered MXenes can solely be facilitated *via* fluorine-related methods. However, MXene terminated with –F group shows an inert property, damaging the electrical conductivity suggesting not favorable for catalyst. Thus, surface cleaning from the –F group is expected to result in a significant catalyst ability

improvement of MXenes. Li *et al.* [93] reported that the fluorine-free Ti_3C_2Tx nanosheets with ~50–100 nm lateral size achieved a high NH_3 yield and an FE of 36.9 $\mu g\ h^{-1}\ mg_{cat.}^{-1}$ and 9.1%, at −0.3 V *vs.* RHE in the 0.1 M HCl environment. The size effect and fluorine-free properties turned the performance of $Ti_3C_2T_x$ around two times higher than that of a fluorine-based treatment [93]. In a more recent case, supported by the DFT calculation results from Johnson *et al.* [91] and Xia *et al.* [92], the bond length of N_2 was slightly larger in F−terminal groups than that of O−containing terminal groups. Ding *et al.* [94] investigated the effect of F−terminated $Ti_3C_2T_x$ MXene in N_2 fixation. They found that a $Ti_3C_2T_x$ MXene with a medium density of surface-functionalized fluorine terminal groups showed an enhanced NRR electrocatalyst with excellent adsorption and activation of N_2. In aqueous solutions at the ambient environment, the $Ti_3C_2T_x$ catalyst exhibited an NH_3 production rate of $2.81 \times 10^{-5}\ \mu mol \cdot s^{-1} \cdot cm^{-2}$, which corresponded to a partial current density of 18.3 $\mu A \cdot cm^{-2}$ and an FE of 7.4% at −0.7 V *vs.* RHE. These results were substantially similar to $Ti_3C_2T_x$ MXene catalysts but with either higher or lower densities of surface fluorine terminal groups. Therefore, there is a demand to further clarify the surface termination effect of MXenes in N_2 activation and reduction.

An interesting development on heterostructures comprised of MXenes and other types of materials towards the enhanced catalytic ability for N_2 capture and reduction to produce NH_3, such as B [95], C [5], Fe [96], Cu [97], Mo [78], Ni [98], Ru [99,100], Au [77], CuAg [101], MoS_2 [79], ZIF−67 [102], *etc.* have been attempted. Single-atom catalysts (SACs) guaranteed low potential, high mass activity, and great selectivity for MXenes [103]. Incorporation of Cu in MXenes in Cu/Ti_3C_2 nanocomposite could remarkably convert N_2 into NH_3. A high FE of 7.31% in a 0.1 M KOH environment was obtained using Cu/Ti_3C_2 nanocomposite as a catalyst and a high NH_3 production rate of 3.04 $\mu mol\ h^{-1}\ cm^{-2}$ at −0.5 V *vs*. RHE was also successfully achieved. Based on the DFT calculation displayed in **Fig. 6 (a)**, the Cu/Ti_3C_2 had wider conduction and valence bands, as well as a larger Fermi level compared with Ti_3C_2 alone, indicating that element of Cu had an important role in the enhancement of the catalytic activity, N_2 selectivity, and conductivity of Ti_3C_2 [97]. In another case, $Ru@Ti_3C_2$ MXene also showed excellent catalytic performance in a 0.1 M KOH electrolyte environment. It was found that the NH_3 yield reached 2.3 $\mu mol\ h^{-1}\ cm^{-2}$, while the FE was 13.13% at −0.4 V (*vs.* RHE) [100]. MXene nanosheets acted as support, while single-atomic Ru anchored on it played a critical part as electron back-donation centers for N_2 activation, promoted N_2 adsorption and activation, and lowered the thermodynamic

energy barrier of the first hydrogenation step [99]. Au nanoclusters anchored in Ti_3C_2 "web" strengthened the interface adsorption, which became the driving force for lessening the triple $N\equiv N$ bonds (evidenced from TPD profiles), and later reduced the activation energy barrier *via* effective stabilization of N_2H^* species and destabilized $NH_2NH_2^*$ under an alternative pathway as illustrated in **Fig. 6 (b) and (c)** [77]. To obtain a highly efficient catalyst process, proper choice of which kind of MXenes and SACs is essential. In most cases, the studies for SACs that incorporate MXenes were mainly focused on F−, O− and OH− functionalized MXenes. N−functionalized MXenes are indeed applicable, and they are even more suitable to anchor the transition metal atoms due to much-enhanced stability. According to a theoretical study, MXenes can dissociate N_2 with a low energy barrier; therefore, the N−functionalization can be easily achieved by heating bare MXenes in the N_2 atmosphere. The catalytic activity of TM anchored N−functionalized MXenes was also dramatically enhanced by injecting some electrons [104]. Moreover, most SACs could bind with Nb_2CN_2 strongly through a TM−3N configuration. Importantly, TM−Nb_2CN_2 presented high selectivity to NRR by blocking the hydrogen adsorption and preventing the HER. Moreover, the scaling relationship and Bader charge analysis provided an insightful understanding of the mechanism for NRR on SACs anchored on 2D MXenes [72].
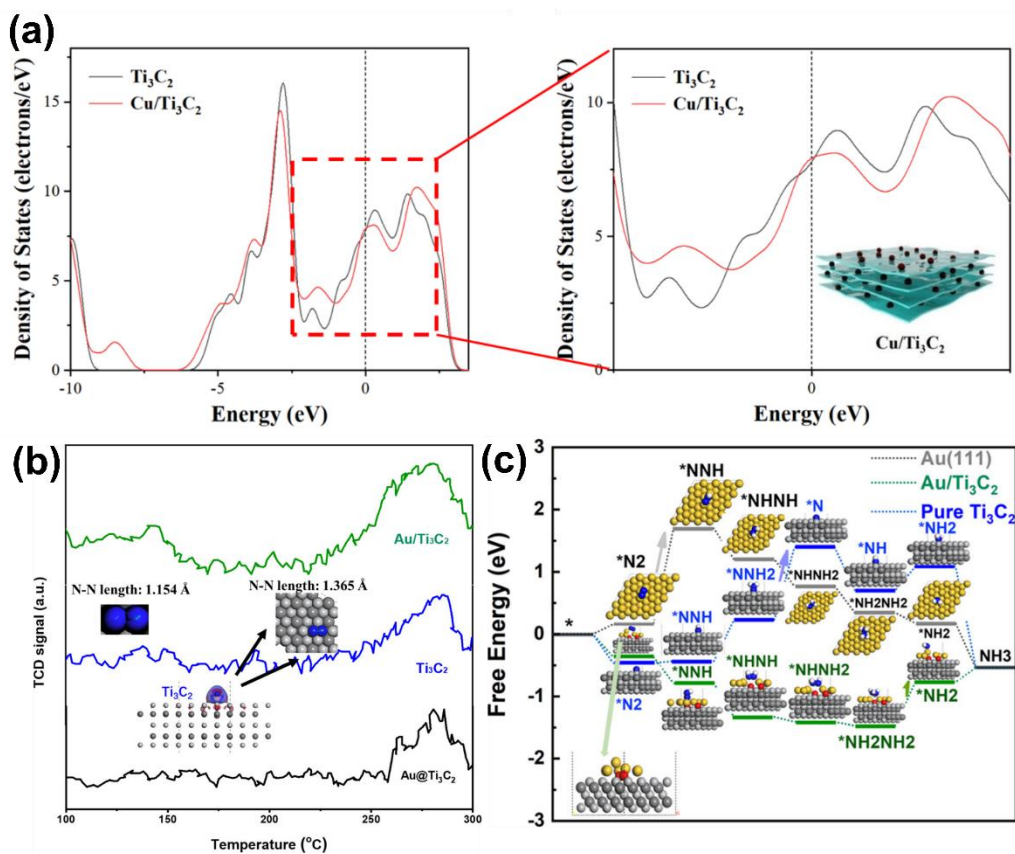
Fig. 6 (a) DOS of the Ti_3C_2 and Cu/Ti_3C_2 composite materials. Adapted from [97]. Copyright 2021 Wiley-VCH Verlag GmbH & Co. (b) N_2−TPD profiles of Ti_3C_2 (blue line), $Au@Ti_3C_2$ (black line), and Au/Ti_3C_2 (green line). (c) Free energy profile for various NRR pathways on Au(111), Ti_3C_2, and Au/Ti_3C_2 samples. Au, N, H, and O atoms are shown in the order golden, blue, white, and red. Reproduced with permission from [77]. Copyright 2020 American Chemical Society.

As Ru and Au are expensive metals, their role could be alternatively substituted by Ti, *i.e.*, Ti incorporated−Mo_2CO_2 ($Ti@Mo_2CO_2$ nanocomposite) could efficiently perform N_2 transformation into NH_3 *via* different reaction mechanisms without bringing a more negative limiting potential [78]. Not only as a single element, but the binary up to quaternary compounds combined with MXenes could also enhance catalytic performance. For instance, $CuAg/Ti_3C_2$ nanocomposite-based-catalyst exhibited remarkable performance for electrochemical synthesis of NH_3 under ambient conditions. In an environment of 0.1 M KOH solution at an applied potential of −0.5 V *vs.* RHE, the catalyst performance achieved an FE and NH_3 production rate of

9.77% and 4.12 μmol cm^{-2} h^{-1}. It was well noted that excellent electrical conductivity and fast electron transport played an essential role in enhancing electrocatalytic reaction in the CuAg/Ti$_3$C$_2$ system [101]. From these significant findings, research work can intensify the exploration of binary and ternary or high entropy metals alloys anchored on MXenes.

The addition of any tandem element or nanoparticles can modify the surface termination of MXene nanosheets achieving high surface area and catalytic reactivity of the NRR for electrochemical conversion into NH$_3$. For example, in the MXene/TiFeO$_x$−700 nanocomposite, where the Fe was decorated in the MXenes [96], the surface development was achieved by ironing inactive F*/OH* terminals to expose more active sites in the surface of the MXenes nanosheet. Here, the element Fe attached to the surface of the MXenes nanosheet could reduce the surface work function. The Fe−induced chemical changes on the MXene surface and strong coupling interactions between Fe and Ti species would improve the surface catalytic reactivity of MXene. The optimal catalyst performance of MXene/TiFeO$_x$−700 nanocomposite was an NH$_3$ yield rate of 2.19 μg h^{-1} cm^{-2} (21.9 μg h^{-1} mg$_{cat.}$$^{-1}$) and FE of 25.44%, which outpaced many electrocatalysts (see **Fig. 7 (a)-(f)**) [96]. By means, the prediction of N$_2$ activation will be at the edge site and is thus rational to switch the catalytically active sites from the basal plane of MXenes to the edge metal. Co−doping with N and S dopants in Ti$_3$C$_2$T$_x$ (NS−Ti$_3$C$_2$T$_x$) induced a synergistic effect in the electron/ion transport capacity and increased the active catalytic sites. Precisely, the pyridine N$_2$ doping of NS−Ti$_3$C$_2$T$_x$ successfully adjusted the catalytically active sites to the edge metal as the presence of thiophene sulfur was mainly located at the edge [105]. The research outcome is speculated to guide a new research avenue on synthesizing non-metals doping for MXenes.
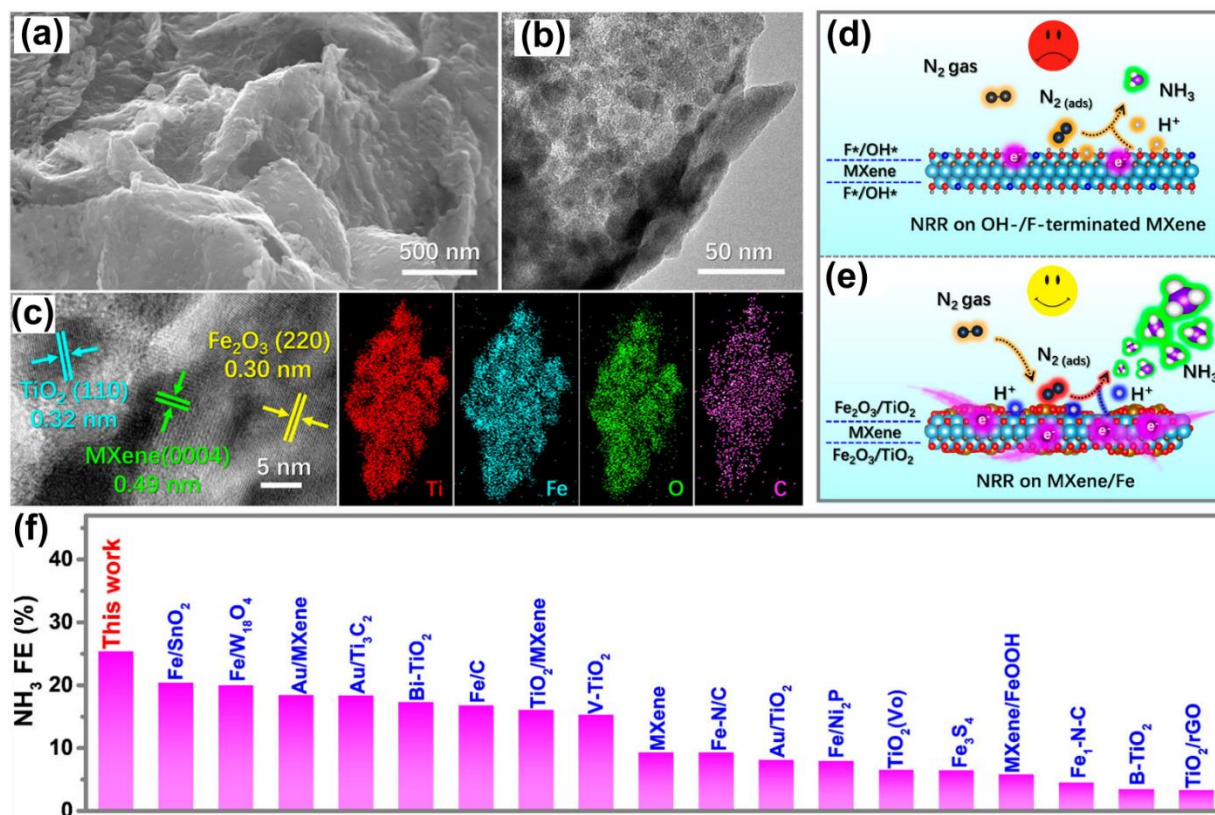
Fig. 7 (a) SEM, (b) TEM, and (c) HRTEM images of MXene/TiFeO$_x$−700 and corresponding EDXS element mapping image of the MXene/TiFeO$_x$−700 nanosheet. (d,e) Schematic illustration for the electrochemical reduction of N$_2$ to NH$_3$ by MXene catalyst and MXene/TiFeO$_x$−700 catalyst. (f) Comparison of Faradaic efficiencies of MXene/TiFeO$_x$−700 with the reported MXene−, Fe−, and Ti−based catalysts. Reproduced with permission from [96]. Copyright 2020 American Chemical Society.

Like the fact that the MXene contained thermodynamically metastable marginal transition metal atoms, and by combining oxygen-vacancy-rich TiO$_2$ nanoparticles with the Ti$_3$C$_2$T$_x$ nanosheets (TiO$_2$/Ti$_3$C$_2$T$_x$) *via* one-step ethanol-thermal treatment has substantially improved the catalytic activity [79], the oxygen vacancies served as the main active sites for NH$_3$ production. The TiO$_2$ nanoparticles could enhance the specific surface area of the Ti$_3$C$_2$T$_x$, showing improvement of the NH$_3$ yield rate to about 32.17 µg h^{-1} mg$_{cat.}^{-1}$ and at −0.55 V *vs.* RHE, then giving rise to an FE of 16.07% at −0.45 V *vs.* RHE in 0.1 M HCl. Moreover, a MnO$_2$−decorated Ti$_3$C$_2$T$_x$ MXene (MnO$_2$–Ti$_3$C$_2$T$_x$) was proposed as a highly active electrocatalyst for the NRR with strong durability proven by N$_2$ yield retention over 90%. It resulted in a high

NH$_3$ yield and FE of 34.12 µg h^{-1} mg$_{cat.}$$^{-1}$ and 11.39%, which was achieved at −0.55 V *vs.* RHE in a 0.1 M HCl environment. DFT investigation as a versatile tool is further used to track down adsorption mechanisms at a molecular level. As a result, the surface of the Mn element was able to serve as an active site to adsorb and activate the inert N$_2$ molecules followed by a distal pathway in the process of NRR, as illustrated in **Fig. 8 (a)-(d)** [106]. Furthermore, MXenes as 2D materials could be combined using other materials (0D, 1D, 2D, and 3D) to bolster their functionality, in particular, to transform N$_2$ into NH$_3$. This included 2D-2D hybrid forms of material based-Mxenes, which were earlier reported to provide excellent ability as N$_2$ catalysts. MoS$_2$ nano spots assembled on Ti$_3$C$_2$ MXene, namely 1T−MoS$_2$@Ti$_3$C$_2$, exhibited excellent N$_2$ catalyst activity with an FE and NH$_3$ yield rate of 10.94% and 30.33 µg h^{-1} mg$_{cat.}$$^{-1}$. The 1T−MoS$_2$@Ti$_3C_2$ nanocomposite also showed good stability and durability during the recycling process. The enhancement of catalytic performance of MoS$_2$@Ti$_3$C$_2$ was induced by the synergy effect between those 2D materials; 1T−MoS$_2$ and Ti$_3$C$_2$ MXene [107].

Various materials could be utilized for NRR catalysts, including MXenes-analogous related materials such as transition metal nitrides (TMNs). Kong *et al.* [108] reported that the surface termination of TMNs, such as Mo$_2$N$_6$, is important to determine the NRR process. Similar to that of MXenes, the catalytic performance of Mo$_2$N$_6$ was improved by atomical doping of metal, such as single atom, metal dimer, and heterodiatom pair [108]. Another example was CrN porous microspheres built up by nanocubes (NCs) which were also found as an efficient noble metal-free electrocatalyst for NRR [109]. The CrN enabled an NH$_3$ yield of 31.11 µgh^{-1} mg$_{cat}$$^{-1}$ with an FE of 16.6% in 0.1 M HCl electrolyte. VN nanowire on carbon cloth (VN/CC) was also disclosed recently to exhibit high-performance catalysts for NRR under ambient conditions. The electrocatalyst of this material achieved a high NH$_3$ yield of 2.48 x 10^{-10} mol^{-1}s^{-1}cm^{-2} and an FE of about 3.58% at −0.3 V Vs. RHE in 0.1 M HCl. These outperform results for N$_2$ fixation under ambient conditions were even better than those obtained under high temperatures and/or pressure [110]. **Table 1** shows the experimental works on MXenes and MXene-based nanocomposites for electrocatalytic NRR, including the reaction pathway.
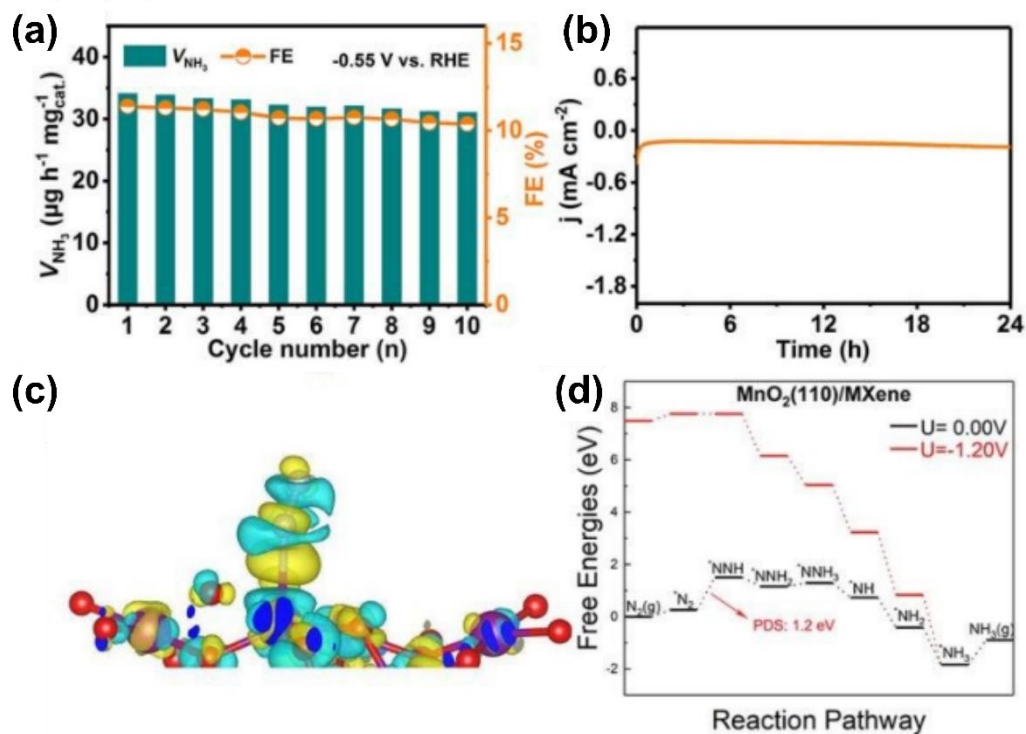
Fig. 8 (a) Stability test of $MnO_2-Ti_3C_2T_x$ during repeated NRR at -0.55 V in N_2-saturated electrolytes. (b) Time-dependent current density curve of $MnO_2-Ti_3C_2T_x$ /CP at -0.55 V for 24 h in N_2-saturated electrolytes. (c) Deformation charge density plot of $MnO_2-Ti_3C_2Tx$ heterostructure absorbing with N_2 molecule. (d) Gibbs energy profile for the N_2 reduction process is performed on the $MnO_2(110)-$MXene surface through the traditional distal pathway. Reprinted with permission from [106]. Copyright 2019 Royal Society of Chemistry.

Table 1. Experimental research on MXenes and MXene-based nanocomposites for electrocatalytic nitrogen reduction.

Catalyst	Electrolyte, membrane, cell	Conditions	NH_3 yield	FE (%), potential *vs*. RHE	N_2 reduction mechanism	By-product	Ref.
$Ti_3C_2T_x$ (T= F, OH) MXene nanosheets	0.1 M HCl, Nafion 211, H−type cell	RT, 1 atm	20.4 µg h^{-1} $mg_{cat.}^{-1}$	9.3% at -0.4 V	Distal pathway	N_2H_4	[81]

Cr_3C_2@C nanofiber	0.1 M HCl, Nafion, H−type cell	RT, 1 atm	23.9 µg h^{-1} $mg_{cat.}^{-1}$	8.6% at −0.3 V	Distal pathway	N_2H_4	[83]
MnO_2−decorated $Ti_3C_2T_x$ (T=F, OH)	0.1 M HCl, Nafion, H−type cell	RT, 1 atm	34.12 µg h^{-1} $mg_{cat.}^{-1}$	11.39% at −0.55 V	Distal pathway	N_2H_4	[106]
$Ti_3C_2T_x$ MXene nanosheets	0.01 M HCl, Nafion 211, H−type cell	RT, 1 atm	4.72 µg h^{-1} cm^{-2}	4.62% at −0.1 V	Distal pathway	N_2H_4	[73]
Fluorine-free $Ti_3C_2T_x$ (T= O, OH)	0.1 M HCl, Nafion 117, H−type cell	RT, 1 atm	36.9 µg h^{-1} $mg_{cat.}^{-1}$	9.1% at −0.3 V	No investigation	N_2H_4	[93]
Au/Ti_3C_2	0.1 M HCl, Nafion 117, H−type cell	RT, 1 atm	30.06 µg h^{-1} $mg_{cat.}^{-1}$	18.34% at −0.2 V	Alternating pathway	N_2H_4	[77]
TiO_2/$Ti_3C_2T_x$	0.1 M HCl, Nafion, H−type cell	RT, 1 atm	26.32 µg h^{-1} $mg_{cat.}^{-1}$	8.42% at −0.6 V	No investigation	N_2H_4	[111]
Oxygen-vacancy-rich TiO_2/$Ti_3C_2T_x$	0.1 M HCl, Nafion 211, H−type cell	RT, 1 atm	32.17 µg h^{-1} $mg_{cat.}^{-1}$	16.07% at −0.45 V	Distal pathway	N_2H_4	[79]
Single-atomic Ru−modified Mo_2CT_x MXene	0.5 M K_2SO_4, Nafion 211, H−type cell	RT, 1 atm	40.57 µg h^{-1} $mg_{cat.}^{-1}$	25.77% at −0.3 V	Alternating pathway	N_2H_4	[99]
Ru@MXene	0.1 M KOH, RDE−type cell	RT, 1 atm	2.3 µmol h^{-1} cm^{-2}	13.13% at −0.4 V	Distal pathway	N_2H_4	[100]

Surface-engineered Ti$_3$C$_2$	0.1 M KOH, Nafion H−type cell	20 °C, 1 atm	1.71 μg h^{-1} cm^{-2}	7.01% at −0.2 V	Alternating pathway *via* a diazene-hydrazine pathway	N$_2$H$_4$	[92]
		60 °C, 1 atm	12.46 μg h^{-1} cm^{-2}	9.03% at −0.2 V			
MXene/TiFeO$_x$	0.05 M H$_2$SO$_4$, Nafion 117, H−type cell	RT, 1 atm	21.9 μg h^{-1} mg$_{cat.}^{-1}$	25.44% at −0.2 V	No investigation	N$_2$H$_4$	[96]
Ti$_3$C$_2$ MXenes nanoribbons	0.5 M KOH, Nafion, H−type cell	20 °C, 1 atm	14.76 μg h^{-1} mg$_{cat.}^{-1}$	3.1% at −0.5 V	No investigation	N$_2$H$_4$	[84]
Hydroxyl-rich Ti$_3$C$_2$Tx QDs	0.1 M HCl, Nafion, H−type cell	RT, 1 atm	62.94 μg h^{-1} mg$_{cat.}^{-1}$	13.30% at −0.5 V	Distal pathway	N$_2$H$_4$	[86]
1T-MoS$_2$@Ti$_3$C$_2$	0.1 M HCl, Nafion, H−type cell	RT, 1 atm	30.33 μg h^{-1} mg$_{cat.}^{-1}$	10.94% at −0.3 V	No investigation	N$_2$H$_4$	[107]
V$_2$CT$_x$ MXene	0.1 M Na$_2$SO$_4$, Nafion H−type cell	RT, 1 atm	12.6 μg h^{-1} mg$_{cat.}^{-1}$	4% at −0.7 V	Distal pathway	N$_2$H$_4$	[82]
Cu/Ti$_3$C$_2$T$_x$ MXene	0.1 M KOH, RDE−type cell	RT, 1 atm	3.04 μmol h^{-1} cm^{-2}	7.31% at −0.5 V	Distal pathway	N$_2$H$_4$	[97]
ZIF−67@Ti$_3$C$_2$	0.1 M KOH, three-electrode cell	RT, 1 atm	6.52 μmol h^{-1} cm^{-2}	20.2% at −0.4 V	No investigation	n.a.	[102]

N−S−doped Ti$_3$C$_2$T$_x$	0.05 M H$_2$SO$_4$, Nafion 117, H−type cell	RT, 1 atm	34.23 μg h^{-1} mg$_{cat.}^{-1}$	6.6% at −0.55 V	No investigation	N$_2$H$_4$	[105]
Ni nanoparticles/V$_4$C$_3$T$_x$ MXene	0.1 M KOH, Nafion 117, H−type cell	RT, 1 atm	21.29 μg h^{-1} mg$_{cat.}^{-1}$	14.86% at −0.55 V	Alternating pathway	n.a.	[98]
F−terminated Ti$_3$C$_2$T$_x$	0.01 M Na$_2$SO$_4$, Nafion 117, H−type cell	RT, 1 atm	0.1 μmol h^{-1} cm^{-2}	7.4% at −0.55 V	No investigation	n.a.	[94]

4.2 MXenes catalyst for photocatalytic N$_2$ reduction

MXenes behave as likely as metals rather than semiconducting materials; they possess metallic properties, *e.g.,* the absence of bandgap and high conductivity. Consequently, pristine MXenes cannot be utilized as a stand-alone catalyst due to their inability to absorb light and generate photoinduced holes-electrons pair. Although some researchers have demonstrated a tunable bandgap by surface engineering, the bandgap does not satisfy the substantial proportion of solar energy absorption requirement. Alternatively, MXenes are robust supports for visible-light active materials to inhibit charge carrier recombination and act as co-catalyst for capturing more molecular N$_2$. Within this framework, photocatalytic materials with an excellent visible-light absorption ability are highly required to enable MXenes towards N$_2$ reduction to NH$_3$. Qin *et al.* attempted to combine 2D Ti$_3$C$_2$ MXene nanosheets with 0D AgInS$_2$ nanoparticles to form a nanocomposite [80]. The hybrid 0D/2D forms of Ti$_3$C$_2$/AgInS$_2$ nanocomposites could conceivably generate the accumulation of multiple electrons. In this case, the 0D AgInS$_2$ nanoparticle had a large surface area and enabled access to a short charge-migration distance, while the 2D Ti$_3$C$_2$ nanosheet supported large contact areas for capturing N$_2$. It was revealed that the Ti$_3$C$_2$/AgInS$_2$ nanocomposites significantly improved photocatalytic NRR under simulated visible-light irradiation and was an outstanding interfacial charge transferability due to their excellent optical and photo-electro properties. For the first time, Ti$_3$C$_2$/AgInS$_2$ nanocomposites recorded a satisfying performance for N$_2$ fixation in which an NH$_3$ yield rate of 38.8 μmol h^{-1}

$g_{cat.}^{-1}$ under visible light illumination was achieved [80]. From the DFT calculations, N_2 activation of $Ti_3C_2/AgInS_2$ nanocomposites led to high adsorption energy ($E_{ad} = -5.20$ eV) [80].

A combination of MXenes with other 2D materials to enhance the NRR electrocatalyst performance was found in the 2D/2D Ti_3C_2/N−defect g−C_3N_4 heterostructure. The referred combination possessed highly enhanced photocatalytic N_2 fixation activity, with an NH_3 yield rate of 5.792 mg h^{-1} $g_{cat.}^{-1}$ and retention yield over 80% [55]. Its heterostructure was fabricated by filling the oxygen terminals of Ti_3C_2 in the N−defects of g−C_3N_4 to form C–O–Ti interactions. The construction of the heterointerface and the introduction of N−defects adds to rapid interfacial charge transfer to the active sites. The mechanism study of photocatalytic N_2 fixation in these heterostructures revealed that the redox circle's evolution originated from the multi-valence Ti species during the N_2 adsorption, activation, and dissociation process. The exposed edge Ti in the Ti_3C_2 was confirmed to be the active site for N_2 adsorption and activation, and these Ti active sites enabled the desirable NRR selectivity by suppressing the competing HER [55].

The modification of the band structure of MXenes through proper combination with other elements and materials held a vital role in enhancing their photocatalyst functionality and efficient charge transfer mechanism in the conversion of N_2 to NH_3. A hydrothermal approach reported this issue in 1D/2D CdS nanorod@Ti_3C_2 MXene (CdS@Ti_3C_2) nanocomposites [112]. CdS demonstrated semiconducting properties being a suitable band structure and superior electronic reduction capability that efficiently lengthen the light absorption range and enhance photocatalytic performance of Ti_3C_2. Likewise, the CdS@Ti_3C_2 showed an excellent photocatalytic N_2 fixation rate of 293.06 μmol L^{-1} h^{-1}, photocatalytic HER rate of 63.53 μmol h^{-1}, and apparent quantum efficiencies (AQE) of 2.28% and 7.88%, which was higher than pure CdS and another CdS−based nanocomposite, *e.g.*, CdS@Pt (**Fig. 9 (a)**). Moreover, CdS@Ti_3C_2 nanocomposite also obtained great long-term stability under simulated sunlight irradiation during the photocatalyst process, evidenced by a stable photocurrent as displayed in **Fig. 9 (b)**.

An in-depth insight into the N_2 conversion reaction pathway should be an area of interest, besides the well-established charge separation and transfer during the photoreduction N_2 mechanism (see **Fig. 9 (c)**). Qin *et al.* [113] investigated the possible fixation pathways on Ti_3C_2−QD/Ni−MOF nanosheets. The Gibbs free energy and the corresponding N–N bond length of the N_2 fixation pathways on the Ti_3C_2−QD/Ni−MOF nanocomposites surface are shown in **Fig. 9 (c)-(d)**. N_2 fixation started from the activation of the energy barrier of 0.74 eV, which led to N–

N bond elongation from 1.098 to 1.118 Å. After that, the electrons transfer occurred from the d−orbital of Ni sites to the N≡N triple bond. The reaction proceeded *via* the distal hydrogenation pathway, which offered a more straightforward and selective hydrogenation process followed by more stretch of N–N bond from 1.196 to 1.266 Å until the release of the first NH_3 molecule. The abundant intermediate of the N_2H_y was found as supporting evidence of FTIR.
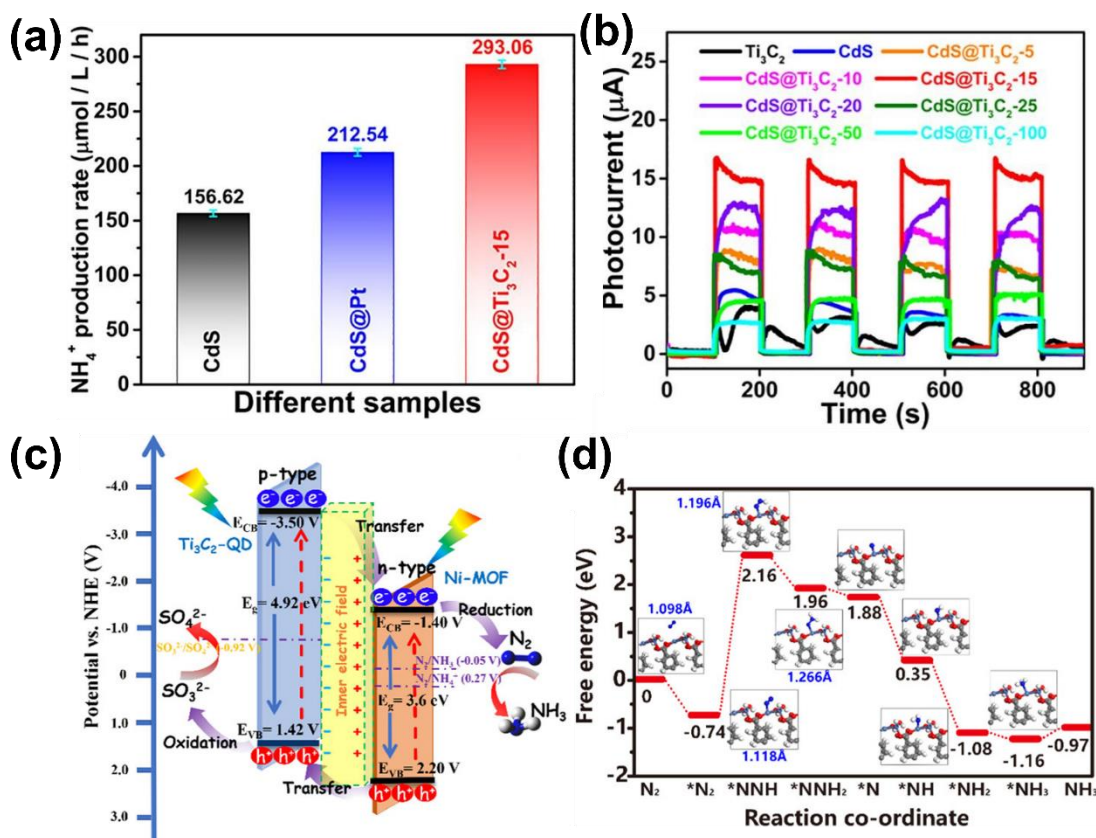

Fig. 9 (a) The NH_4^+ production rate and (b) photocurrent response of CdS NRs, CdS@Pt, and CdS@Ti$_3$C$_2$−15 composite under simulated solar light illumination. (c) Energy band positions of Ti$_3$C$_2$−QD/Ni−MOF. (d) Change in the N−N bond length and the free-energy change against the reaction coordinate during the reaction process. (a) and (b) are reprinted with permission from [112]. Copyright 2021 Elsevier. (c) and (d) are reproduced with permission from [113]. Copyright 2020 American Chemical Society.

MXenes have been well-known for their vast surface area, excellent electrical conductivity, and effective chemisorption/activation of N_2 molecules, which are prominent properties to improve the photocatalytic NH_3 synthesis performance of the P25 and g−C$_3$N$_4$ photocatalysts for as efficient co-catalysts [114,115]. The combination of MXenes with those photocatalysts

increased the production yield of NH_3 to multi-folds compared to the pristine photocatalysts under the same full-spectrum light irradiation. An in-depth investigation revealed the immense contribution of oxygen vacancies and exposed edge Ti of $Ti_3C_2T_x$ MXenes as an active center for N_2 absorption and activations, which led to excellent selectivity and a reduced competing HER. An in-depth investigation revealed the immense contribution of oxygen vacancies and exposed edge Ti of $Ti_3C_2T_x$ MXenes as an active center for N_2 absorption and activations, which led to excellent selectivity and a reduced competing HER. The photocatalyst tandem should be adequately designed because not all photocatalysts are well-suited with MXenes. Following considerations should be justified: (i) The position of the valence band should be lower (more positive) than the potential of oxygen evolution, and the position of the conduction band should necessarily be higher (more negative) than the reduction of N_2 hydrogenation potential. (ii) It is important to design photocatalysts with small bandgap energy, preferably within the visible light energy, to optimize natural sunlight utilization. However, the bandgap structure should meet the oxidation and reduction potentials mentioned above. (iii) The matching band structures between photocatalysts and MXenes will facilitate the charge transfer process at the interface. It should be noted that MXenes are mainly metals whose work functions are mostly higher (more negative) than many photocatalysts. Therefore, the resulting band structures of the composite should not inhibit the N_2 hydrogenation reaction. The recent investigation of MXenes as co-catalyst and support materials for N_2 photoreduction and conversion to NH_3 is compiled in **Table 2**.

Table 2. MXene-based nanocomposites for photocatalytic nitrogen reduction.

Catalyst	Conditions	Scavenger	Light source	Testing method	NH_3 yield rate	Stability (yield retention)
AgInS$_2$/MXene [80]	N_2 atmosphere, RT, and AP	CH_3OH	300 W Xenon lamp	Indophenol blue	3.88 μmol h^{-1} g$_{cat.}^{-1}$ (AQY=0.07%) ($\lambda > 400$ nm)	15 h (~73%)
RuO$_2$−loaded TiO$_2$−MXene [116]	N_2 gas (50 ml/min), RT, and AP	No	Xenon lamp irradiation (100 mW cm^{-2})	Salicylic acid-hypochlorite	45 μmol L^{-1} h^{-1} g$_{cat.}^{-1}$	6 h (~84.4%)

$Ti_3C_2-QD/Ni-MOF$ [113]	N_2 gas (10 mL/min), 25°C, AP	Na_2SO_3	300 W Xenon lamp (simulated solar light irradiation)	Nessler's reagent	88.79 μmol h^{-1} g$_{cat.}$$^{-1}$ (AQY=0.139%)	9 h (~98%)
$Ti_3C_2T_x/TiO_2$ hybrid structures [117]	N_2 gas (30 mL/min), 25°C, AP	No	Xenon lamp (250 mW cm^{-2})	Nessler's reagent Indophenol blue Ion chromatograph	422 μmol h^{-1} g$_{cat.}$$^{-1}$ ($\lambda > 320$ nm) (AQY=0.07%) 50 μmol h^{-1} g$_{cat.}$$^{-1}$ ($\lambda > 630$ nm) (AQY=0.05%)	10 (~90%)
CdS nanorod@Ti_3C_2 MXene [112]	N_2 gas (30 mL/min), RT, AP	CH_3OH	300 W Xenon arc lamp	Nessler's reagent	293.06 μmol L^{-1} h^{-1} (AQY = 7.88%)	6 h (~97.94%)
$Ti_3C_2/N-$defect g$-C_3N_4$ [115]	N_2 gas (30 mL/min), 35°C, AP	CH_3OH	300 W Xenon lamp	Nessler's reagent	5.792 mg h^{-1} g$_{cat.}$$^{-1}$	18 h (~83%)
Co/MXene/TiO_2 [118]	N_2 gas (80 mL/min)	No	300 W Xenon lamp	Nessler's reagent	110 μmol h^{-1} g$_{cat.}$$^{-1}$	18 h (~99%)
P25/Ti_3C_2 [114]	N_2 gas (200 mL/min), RT, AP	CH_3OH	300 W Xenon lamp	Ion chromatography	43.44 μmol. g$_{cat.}$$^{-1}$	No investigation

AQY = Apparent quantum yield
RT = Room temperature
AP = Atmospheric pressure

4.3 MXenes-derived catalysts for N_2 reduction to NH_3

The chemical composition of MXenes is diversified and versatile, owing to being flexibly synthesized from one or two transition metal elements combined with carbide or nitride and

terminated with surface functional groups. According to the recent report, over 150 compositions have been experimentally and theoretically explored MXenes [22,70,119]. With this particular property, MXenes can be potentially derived into many compelling catalysts for NRR as its extensive application in energy storage and general catalysts are getting real. Despite the fact that it remains in an early stage of development, we present the latest progress of MXene-derived catalysts for NRR herein.

As one of the MXenes-derived catalysts, the $TiO_2@C/g-C_3N_4$ heterojunction was thermally derived from $Ti_3C_2T_x$ coupled *in situ* with $g-C_3N_4$ nanosheets, as shown in **Fig. 10 (a)**. Derivatives TiO_2 morphology consisted of the aggregated small-sized bipyramids and large-sized nanocuboids. The heterojunctions exhibited numerous significances, such as abundant surface defects, high electron-donating ability, adequate light-harvesting ability, exquisite charge transport properties, and strong N_2 activation ability having an NH_3 production rate of 250.6 µmol $g_{cat.}^{-1}$ h^{-1} under visible light irradiation, which suggested a suitable N_2 electrocatalyst (**Fig. 10 (b)**) [54]. Another work from Zhao *et al.* explored material derivation from MXenes: anatase and rutile phases of TiO_2. They have successfully combined the TiO_2 and carbon forming TiO_2/carbon nanocomposites with a sandwich design from the annealing process of MXene. The TiO_2 phase could be easily turned into anatase and rutile phases. With the aid of 0.1 M Na_2SO_4 electrolyte, anatase TiO_2/C composites resulted in excellent N_2 catalytic performance compared to the rutile TiO_2/C fabricated regardless of a similar method used. The NH_3 yield rate of 14.0 µg h^{-1} cm^{-2}, high FE of 13.3% at −0.2 V *vs*. RHE, and excellent electrochemical stability were clearly achieved. The authors attributed the sandwich architecture of the well-dispersed anatase TiO_2 nanoparticles on the surface of carbon layers to improve the conductivity of TiO_2. Additionally, the composite design enabled exposure of the active sites and increased the N_2 catalytic activity of anatase TiO_2/C composites. According to DFT calculations, the improvement of catalytic activity was mainly caused by the energy barrier of the most steps surface of the anatase TiO_2 that relatively lower than that of rutile TiO_2, marking NRR performance for anatase TiO_2/C composites way better than the rutile TiO_2/C composites [120].

The thermal calcination warrants the successful derivation of MXenes with some interesting surface properties. Recently, oxygen vacancy-rich C/TiO_2 ($OV-C/TiO_2$) was successfully fabricated using a one-step calcination approach by Ti_3C_2 MXene as the precursor [121]. The derived morphology comprised of TiO_2 layered structures decorated with a regular

octahedral structure with sizes of 100−300 nm was confirmed by SEM in **Fig. 10 (c)**. The NH$_3$ yields of Ti$_3$C$_2$−derived OV−C/TiO$_2$ were much higher than those on commercial anatase TiO$_2$ and P25 catalysts, established by more efficient chemisorption of N$_2$ compared to commercial anatase TiO$_2$. The work also investigated the effect of proton sources on NH$_3$ production rates. Employing H$_2$O as the only electrolyte gave 41.00 µmol g$_{cat.}^{-1}$ h^{-1} while adding CH$_3$OH into the system boosted the yield rates to 84.00 µmol g$_{cat.}^{-1}$ h^{-1} (**Fig. 10 (d-e)**). DFT calculations further suggested that excellent N$_2$ conversion to NH$_3$ through a Gibbs free energy released in OV−C/TiO$_2$ leading alternating pathway with low energy barriers on the oxygen vacancy of the TiO$_2$ surface **Fig. 10 (f)**.
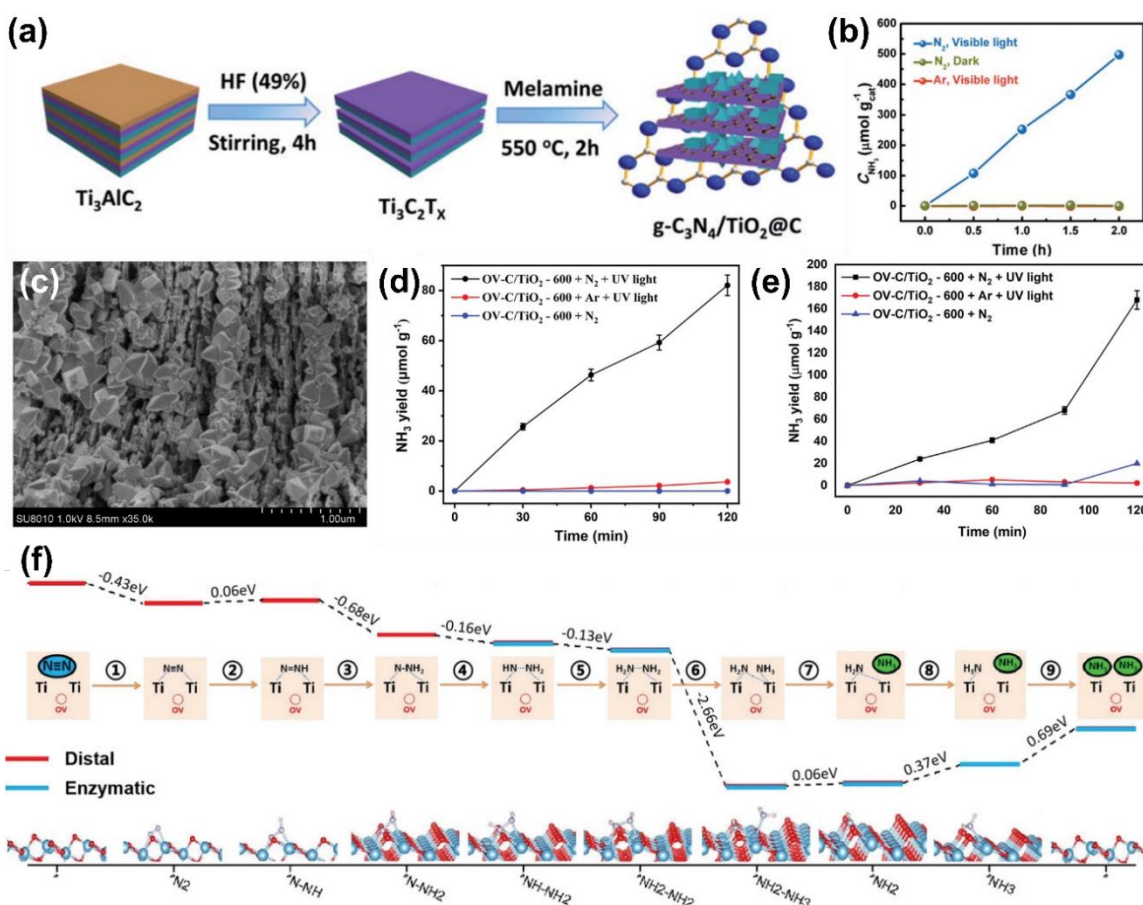

Fig. 10 (a) Schematic illustration of the synthesis process and (b) NH$_3$ production under visible light irradiation ($\lambda > 420$ nm) of TiO$_2$@C/g−C$_3$N$_4$. Reproduced from [54] with permission. Copyright 2018 Royal Society of Chemistry. (c) SEM images of SEM images of OV−C/TiO$_2$−600. Control experiments of NH$_3$ generations for OV−C/TiO$_2$−600 with (d) H$_2$O as the proton source

and (e) CH_3OH as the proton source. (f) Reaction pathway for the N_2 conversion into NH_3 in the site of oxygen on the surface of TiO_2. Reprinted with permission from [121]. Copyright 2021 Wiley-VCH Verlag GmbH & Co.

As previously mentioned, various material derivation was found depending on the parent material of MXenes. TiO_2 may become one of the derivation materials from Ti−based MXenes that widely explored so far, especially for NRR applications. A series of 3d, 4d, and 5d−transition metal M_2C (M = Sc, Ti, V, Cr, Mn, Fe, Zr, Nb, Mo, Ta, and Hf) MXenes were named promising for the NRR applications [122]. Thus, as likely Ti−based MXenes derived into TiO [121], V−based MXenes into V_2O_5 [123], other types of MXenes as parent materials also could be possible derived into various materials prior to N_2 catalyst application. To put into context, MnO_2 ─from Mn−based MXenes reported improving the N_2 catalytic ability of $Ti_3C_2T_x$ [106]. A recent report worked on the possibility of the Nb based−Mxenes derivatives, such as Nb_2O_5, to be utilized as N_2 catalysts. In later exploration, 2D MXene-derived niobium pentoxide/carbon/niobium carbide/graphite-like carbon nitride ($Nb_2O_5/C/Nb_2C/g−C_3N_4$) heterojunctions were found promising as photocatalysts for NRR in water. In such a case, Jiang et $al.$ [68] prepared the $Nb_2O_5/C/Nb_2C/g−C_3N_4$ heterojunctions using uniformly growing Nb_2O_5 on Nb_2C and was followed by the formation of $g−C_3N_4$ nanosheets in $situ$ on $Nb_2O_5/C/Nb_2C$. The optimized $Nb_2O_5/C/Nb_2C/g−C_3N_4$ sample gave a high NRR of 0.365 mmol h^{-1} $g_{cat.}^{-1}$, which was 9.1 times larger than MXene derived $Nb_2O_5/g−C_3N_4$ composite alone. The catalytic activity improvement of $Nb_2O_5/C/Nb_2C/g−C_3N_4$ could be associated with the enhanced photogenerated electron-hole separation efficiency attributable to the short-range directional charge transmission over the close interfacial contact between Nb_2O_5 and Nb_2C. The N_2 photo fixation process may have influenced the Schottky junction formed at the Nb_2O_5 and Nb_2C interfaces. Furthermore, with the adjusted pH ~9 made by NaOH solution, the NRR efficiency of $Nb_2O_5/C/Nb_2C/g−C_3N_4$ reached 0.927 mmol h^{-1} $g_{cat.}^{-1}$ or 2.5 times larger than without adjusting treatment.

Mo−based material is a viable candidate for the efficient electrocatalytic NRR [124]. MXene containing Mo atom can be potentially derived into a Mo−based catalyst. Although no report about it yet, its performance could be expected according to the preceding work by Wang et $al.,$ as they combined the MoO_2 nanoparticles with reduced graphene oxide (MoO_2/RGO) for ambient condition, electrocatalytic NRR presented a high activity with an NH_3 yield of 37.4 μg h^{-1} $mg_{cat.}^{-1}$ and an FE of 6.6% at −0.35 V ($vs.$ RHE) in 0.1 M Na_2SO_4 environment [125]. With

the rapid growth of research on MXene derivatives, a more informative and systematic investigation of their N_2 reduction properties is exciting and worth waiting. A summary of MXene-derived N_2 catalyst is compiled in **Table 3**.

Table 3. MXene-derived catalysts for efficient nitrogen reduction.

Type of MXenes	Derivatives	Synthesis method	Derived morphology	NH_3 yield	Ref.
$Ti_3C_2T_x$ MXene	$TiO_2@C/g-C_3N_4$	One-step calcination	TiO_2 nanocrystals composed of the aggregated small-sized bipyramids and large-sized nanocuboids	250.6 μmol $g_{cat.}^{-1}$ h^{-1}	[54]
$Ti_3C_2T_x$ MXene	Anatase TiO_2/C Composites	Thermal annealing	2D carbon layers with embedded TiO_2 particles (sandwich architecture)	14.0 μg h^{-1} cm^{-2}	[120]
Nb_2CT_x	$Nb_2O_5/C/Nb_2C/g-C_3N_4$	CO_2 oxidation at 850 $^{\circ}$C	Nb_2C layered with decoration of Nb_2O_5 nanocrystal	0.365 mmol h^{-1} $g_{cat.}^{-1}$	[126]
$Ti_3C_2T_x$ MXene	Oxygen vacancy-rich C/TiO_2	One-step calcination	TiO_2 octahedral structure- decorated 2D layered structures	84.00 μmol $g_{cat.}^{-1}$ h^{-1}	[121]

4.4 General strategies to improve the NRR performance of MXenes and their derivatives

The comprehensive discussions on the recent advances of MXenes and their derivatives for N_2 reduction catalysts have shown a straightforward demonstration of their promising performance. Herein, we include the general strategies which may further improve the electrocatalytic and photocatalytic performances for NRR based on MXenes derivatives as listed below:

- Doping; various doping has been recently used to improve the electrocatalytic performance of MXenes. For instance, metal atoms could change the relevant reaction mechanism (from Volmer-Heyrovsky to Volmer-Tafel), promote electron redistribution on the surface of the

MXenes, and thus enhance the properties required for NRR catalytic, such as conductivity, stability, and adsorption [127]. As for photocatalyst, doping could solve the problem by easy recombination of photoelectrons and holes, improving its light-harvesting by suitable bandgap adjustment, and improving surface functional groups [128].

- Composing; combining MXenes with other materials as composite forms could improve the electro- and photo-catalyst performance of MXenes. Interfacial coupling between MXenes and the companient materials is pivotal because it can facilitate the charge carriers' separation/transfer. Composing MXenes with other materials also enabled to improve the stability [129].

- Low dimension formation, size, and morphology; enhancement of the NRR activity of MXenes in most cases have been promoted due mainly to more specific surface areas for interfacial interaction between materials and molecular N_2. Therefore, a suitable choice of low dimension formation, size, and morphology are important to determine the catalytic properties. For instance, in quantum dot form, MXenes have abundant active sites that allow the development of efficient NRR catalysts.

- Surface engineering; the surface hydroxyl groups were considered to effectively facilitate the electron transfer and promote the adsorption and activation of dinitrogen [92].

- Strain engineering; this method was found feasible to improve the photocatalytic performance of MXenes since train engineering tuned the bandgap and the effective mass and thus electron's mobility [130]. In general, strain engineering could vary the electronic structures of MXenes, further reflecting on their optical properties, which were essential for photocatalytic performance [131]. Strain also could be used to tune the type of transition, such as type-I/type II transition in MXenes, which then affect the optical properties of MXenes [132].

5. MXenes and MXenes-derived catalysts preparation

Following the insightful discussion on the MXene and MXene derivatives application for NRR catalysts, it is essential to focus on their preparation protocols to accelerate the research progress further. Numerous fabrications methods such as mechanical or ultrasonic mixing, electrostatic self-assembly, hydrothermal and solvothermal treatment, and calcination processes were mainly used to synthesize MXene-based and MXene-derived catalysts [31]. With the increasing demand for MXenes for NRR catalyst applications, we assure there will be extensive synthesis methods of MXenes in various forms such as 0D, 1D, and 3D, other than the 2D form currently explored. Therefore, we overview recent synthesis and properties of MXenes for N_2 catalyst applications, including single flakes MXenes from 3D to 0D structures, MXenes nanocomposites, and MXenes derivatives materials as depicted in **Fig. 11**. The overview of 0D to 3D forms herein is not limited to the forms of Mxenes alone, but several combinations of 0D, 1D, 2D, and 3D forms of tandem materials with general 2D MXenes, *i.e.*, intercalated of 0D and/or 1D tandem materials into 2D MXenes nanosheet.

5.1 Synthesis of 0D MXenes

The 0D MXene consistently exhibits excellent catalyst capability for its high surface free energy and unsaturated coordinated atom within an overly small region, although a skeletal framework should support the utilization to hinder the agglomeration. Up to now, 0D MXenes catalysts have shown encouraging results of the carbon dioxide reduction reaction (CO_2RR), NRR, and HER. The mechanical related or ultrasonic mixing methods were the easiest way to prepare MXenes-based photocatalyst [9] *via* strong mechanical stirring and high-power ultrasonic vibration into various MXenes forms; with 0D is no exception. This method is involved in the top-down method process of synthesis 0D materials [133]. Top-down fabrication is done by breaking or crushing the parent material MXenes into small pieces —later called 0D or quantum nanodot (QDs) as they are in a quantum size regime (the dimensions or sizes of materials are smaller than their characteristic of exciton Bohr radius). Various top-down fabrication methods of 0D MXenes were conducted recently, constituting hydrothermal process, sonication, solvothermal, etc. A study by Xue *et al.* successfully fabricated Ti_3C_2 MXenes QDs *via* a facile hydrothermal method by cutting the bulk Ti_3C_2 MXene as a starting material. This procedure

greatly influenced different morphologies of colloidal Ti3C2 QDs by the reaction temperature [134]. Meanwhile, Lu *et al.* fabricated the Ti_3C_2 QDs through a two-step facile solvothermal route, with bulk Ti_3C_2 as a starting material and oleylamine (OLA) as a surface passivation agent [135]. In addition, Qin *et al.* reported fabricating the $Ti_3C_2T_x$ QDs with high yield (60%) from 2D $Ti_3C_2T_x$ using facile tetramethylammonium hydroxide (TMAOH) reflux-assisted approach [136]. The Ti_3C_2 QDs also have been synthesized *via* ultrasonication of 2D Ti_3C_2 MXenes using the subsequent dispersion process in the dimethyl sulfoxide (DMSO) solution under an N_2−protected environment [137].

On the other hand, the bottom-up method is referred to as the "knit" process of a series of small an/organic molecules or oligomers under a relatively mild condition. The typical bottom-up synthesis methods include chemical oxidation, combustion, hydrothermal/solvothermal, microwave synthesis method, template method, etc. [133]. However, no one previously reported that 0D MXenes were prepared using bottom-up approaches to the best of our knowledge. In most cases, the MXenes are generally 2D materials that act as "starting" to obtain 0D forms by breaking the 2D ones into 0D forms. At this rate, the 0D forms of MXenes could only be found using top-down methods.

The MXenes QDs are possibly combined with various materials to develop a nanocomposite. Different fabrication methods of nanocomposite based-MXenes QDs have been conducted. For instance, g−C_3N_4@Ti_3C_2 QDs nanocomposites were fabricated by a combination of DMSO and hydrothermal sonification process using PEI [138]. In this nanocomposite, the Ti_3C_2 QDs improved the specific surface area of g−C_3N_4 and boosted the active site's density [138]. Another report came with a similar configuration with the addition of TiO_2 to form a 2D/2D/0D nanocomposite, namely TiO_2/C_3N_4/Ti_3C_2 (T–CN–TC) [137]. The nanocomposite was successfully fabricated following several steps of chemical routes; (i) the fabrication of 2D TiO_2 nanosheets with single-layered mesopores *via* hydrothermal-induced solvent-confined monomicelle self-assembly, (ii) synthesis of mesoporous TiO_2/C_3N_4 core-shell nanosheets using the thermal condensation, and (iii) electrostatic assembly of Ti_3C_2 QDs with the C_3N_4 shell, producing the TiO_2/C_3N_4/Ti_3C_2 (T–CN–TC) composite [137]. Zeng *et al.* [139] synthesized an 0D/1D nanocomposite of Ti_3C_2 QDs/Cu_2O nanowire *via* a facile self-assembly method. The Ti_3C_2 QDs in this way could uniformly be distributed on the surface of Cu_2O nanowires. The Ti_3C_2 QDs enhanced the Cu_2O nanowires' stability, increased active sites, and greatly improved the light

adsorption and charge transfer. Also, Ti_3C_2−QDs combined with 2D nickel metal-organic framework (Ni−MOF) were successfully fabricated using a facile self-assembly method forming type II heterojunctions. The nanocomposites exhibited an enhancement of absorption ability and excellent interfacial charge-transfer capabilities [113].

5.2 Synthesis of 1D MXene

The 1D materials refer to the materials preferable to be crystallized in single directions and negligible in 2Ds. The materials include nanorods, nanowire, nanoribbon, and nanotubes. A 2D MXene basically could be tailored into 1D forms to enhance their functionality. The 2D transformation into 1D is quite tricky because the crystal growth direction of MXenes should be able to grow in only one direction and be restricted to the other sides. It is contradictory with the formation nature of MXenes that has general forms of 2D and grows in two directions. Nevertheless, there are always open opportunities in research. Lian *et al.* [140] and Wei *et al.* [84] have successfully fabricated MXene nanoribbons from pristine Ti_3C_2 MXene by continuous shaking treatment in an aqueous KOH solution. In principle, alkali treatment enabled the surface group transformation from –F into –OH, thus increased the rapid adsorption and intercalation of K^+ into the layers. The mechanical shaking treatment increased the diffusion of OH^- and K^+ along the channels of interlamination; it contributed to the O−terminated MXene nanoribbons and thus split MXene nanoribbons from the delaminated sheets [140]. Using a similar method, KOH−assisted treatment, Ti_3C_2 MXene nanoribbons could be fabricated directly using the Ti_3AlC_2 MAX phase. The OH^- could now act as "the scissor" to cut Ti–C bonds, thus fabricated the crack propagating to the edge to form nanoribbons [141]. Moreover, Li *et al.* studied the effect of KOH solution concentration in fabricating Ti_3C_2 MXene nanoribbons. They found that the concentration of KOH solutions was critical to determine the morphology and quantity of Ti_3C_2 nanoribbons [142].

On the other hand, the 2D forms of MXenes with large surface areas have been combined with 1D materials to increase their surface functionality. The 1D/2D CdS nanorod@Ti_3C_2 MXene (CdS@Ti_3C_2) nanocomposites, for example, were prepared in a hydrothermal treatment. In this case, the CdS nanorod with wide optical absorption was placed on the surface of 2D MXenes, enabling the enhancement of the light absorption photocatalytic performance better than pure CdS and another CdS−based nanocomposite such as CdS@Pt [112]. Another result reported by Yu *et*

al. integrated MXenes CrC_2 nanoparticle−embedded carbon nanofiber *via* the electrospinning technique, which then this MXenes-based nanofiber composite was being used for N_2 fixation under ambient conditions [83].

Various reports on 1D/2D MXenes-based heterostructures were done to increase and improve the functionality of MXenes, involving MXenes derivatives, such as MXene-derived heterostructures of nanoribbon-like $Na_{0.23}TiO_2/Ti_3C_2$ and $NaTi_8O_{13}/NaTiO_2$ nanoribbons $/Ti_3C_2$ with its unique sandwich structure [143,144]. Dong *et al.* also managed to fabricate Ti_3C_2 MXene−derived $NaTi_{1.5}O_{8.3}$ nanoribbons and $K_2Ti_4O_9$ nanoribbons through simultaneous Ti_3C_2 oxidation and alkalization [145]. MXene-derived carbon nanotube network that encapsulated CoS_2 nanoparticles ($CoS_2/CNTs/TiO_xN_y$) heterostructure was also successfully synthesized [146].

5.3 Synthesis of 2D MXenes

The 2D MXenes are general forms of MXenes, derived from 3D MAX phases and prepared mainly by selective etching of the A element layers from the 3D MAX phases [147]. Since 2D as an available form of MXenes has been widely discussed in many articles, we focus on the 2D-2D hybrid forms of nanocomposite-based MXenes. The complete guidelines of how MXenes were synthesized and processed were discussed by Gogotsi's group [148]. The 2D/2D nanocomposite was forecasted to be more efficient and more surface reaction sites for the photocatalysis process than 0D/2D and 1D/2D architectures [31]. The 2D-2D hybrid forms of MoS_2 nano spots assembled on Ti_3C_2 MXene, known as $1T−MoS_2@Ti_3C_2$, exhibited excellent N_2 catalyst activity. The $1T−MoS_2@Ti_3C_2$ nanocomposite also presented magnificent stability and durability during the recycling process. The enhancement of catalytic performance of $MoS_2@Ti_3C_2$ was induced by the synergy effect between those 2D materials; $1T−MoS_2$ and Ti_3C_2 MXene [107]. Sun *et al.* also successfully simulated an excellent N_2 photocatalyst of a novel 2D/2D $Ti_3C_2/N−$defect $g−C_3N_4$ heterostructure. The CT−CN nanosheet heterostructure was achieved by filling the oxygen terminals of Ti_3C_2 in the N−defects of CN to form C–O–Ti interactions. The assembly of CN and Ti_3C_2 was done *via* an electrostatic adsorption and heat treatment process [115]. Almost similar to this report, Zhao *et al.* fabricated 2D $g−C_3N_4$ composed of 2D MOFs (cobalt 1,4−benzene dicarboxylate, CoBDC) and $Ti_3C_2T_x$ through an interdiffusion reaction strategy [149]. The 2D/2D heterointerface of ultrathin Ti_3C_2/Bi_2WO_6 nanosheets was reported using *in situ* growth of Bi_2WO_6 nanosheets on the surface of the Ti_3C_2 nanosheets [150].

5.4 Synthesis of 3D MXenes

The 2D MXenes are generally derived from the 3D MAX phase as the parent material. However, 2D MXenes could also be categorized as 3D materials when they crystalized at three growth directions or, the 2D sheet of MXenes was heavily three-dimensionally stacked at vertical direction [75]. Transforming the 2D MXenes into 3D forms could overcome the re-stacking problem, easily control undesirable oxidation, and widen the development horizon of MXenes-based functional materials [151,152]. Unlike graphene, the 3D MXenes macro assembly directly from the individual 2D sheets was tough to achieve the MXenes intrinsic property [151]. It was essential to design a simple and efficient strategy that allowed the easy transformation of 2D into 3D architectures with exposed surface facets without compromising the compositional integrity and inherent stability of MXenes [152].

Zhang *et al.* successfully transformed the 2D $T_3C_2T_x$ Mxenes into 3D carbon-coated $T_3C_2T_x$ architecture, namely 3D tremella-like architecture (T−MXene@C), using self-polymerization of dopamine over the surface of $T_3C_2T_x$ nanosheets as a parent material then treated in freeze-drying and carbonization under an inert air atmosphere. The self-polymerization of dopamine not only enabled the transformation of 2D $T_3C_2T_x$ into 3D tremella-like architecture, but its subsequent carbonization resulted in complete coverage of a thin carbon coating that preserving the structure from both air-oxidation and structural aggregation [152]. Yuan *et al.* succeeded in fabricating the 3D $T_3C_2T_x$ *via* an electrospinning technique coupled with a self-assembly approach [153]. Later, Shang *et al.* fabricated 3D structured hydrogel MXenes using the gelation method from 2D MXene sheets assisted by graphene oxide and reductant [151]. Liu *et al.* proposed a facile strategy to construct 3D hierarchical porous Ti_3C_2/bimetal−organic framework (NiCo−MOF) nanoarchitectures [154]. Hydrogen bonds induced these 2D Ti_3C_2 nanosheets coupled with NiCo−MOF nanoflakes forming 3D nanocomposite films through a vacuum-assisted filtration technique. The 3D forms of MXenes would be easier to realize when they are in the nanocomposite forms, which means they are stuck in a medium binder. To this extent, the MXenes in 0D and/or 2D would be formed in various 3D forms. MXenes stuck in the medium binder are easier to assemble in 3D using varied synthesis methods.

5.5 Synthesis of MXenes derivatives

Research and development of the nanostructures derived from MXenes compounds are still in primitive development. Much effort should be devoted to the architecture design of MXenes derivatives in the future, especially for NRR electrocatalyst applications. Since $Ti_3C_2T_x$ MXenes could be derived into various materials, TiO_2−derived MXene is one of its kind [59]. Tang *et al.* accomplished fabrication of layer-stacked a−TiO_2 by a two-step oxidation route from HF−etched $Ti_3C_2T_x$. The two-step oxidation comprised the hydrothermal treatment prior to calcination to alleviate the abnormal grain growth resulting in a 2D morphology composing a−TiO_2 nanoparticles. The formed nanoparticles were due to the formation of carbon during the hydrothermal oxidation of $Ti_3C_2T_x$, which could hamper mass diffusion through the crystal boundary during calcination [155]. Wang *et al.* fabricated the MXene-derived mesostructured of the TiO_2–graphene composite prepared by oxidizing Ti_3C_2 MXenes with H_2O_2. The obtained TiO_2 was thus mixed with graphene, calcined, and freeze-dried under an argon atmosphere [156]. Instead of TiO_2, Dong *et al.* oxidized and alkalized the HF−etched Ti_3C_2 simultaneously with a mixed solution of NaOH (or KOH) and H_2O_2 to synthesize ultrathin nanoribbons of sodium titanate and potassium titanate under hydrothermal conditions [157]. Moreover, the micron-sized nanoporous V_2O_5 arrays derived from V_2CT_x MXenes through a one-step annealing process were also reported by regulating the temperature and heating rates [157]. Other works include TiO_2@C composites that have been successfully fabricated *via* a ball milling of Ti_2C powders, treated Ti_3C_2 sheets with 30% H_2O_2 at room temperature to synthesize Ti_3C_2/TiO_2−x nanodots, and facile synthesis using hot water (60 °C) to oxidize the Ti_3C_2 to obtain a series of TiO_2/Ti_3C_2@amorphous carbon composites [158].

Choosing a proper fabrication method is necessary to modify the MXenes into their derived materials efficiently. Zhong *et al.* suggested that calcination and hydrothermal oxidation methods were the most fabrication techniques that are widely used in the material derivation of MXenes, particularly for photocatalyst applications [31]. As mentioned, TiO_2 is the most used material derivation of MXenes for N_2 catalyst applications that could be derived by oxidizing CO_2 with Ti_3C_2. Earlier reported that the CO_2 molecule could break the Ti−C bonds in Ti_2C_3, resulting in

the formation of TiO_2. This method could be further improved by carbon- and sulfur-doped TiO_2 *via* sulfur intercalation of Ti_3C_2 and a two-step oxidation process [158]. Kong *et al.* prepared TiO_2/carbon by the high-temperature oxidation process [159], while Huang *et al.* also fabricated TiO_2 derivation from Ti_3C_2 by calcination in a CO_2 atmosphere to form $TiO_2@C$ [128]. In addition to calcination methods, the derivation material of MXenes could also be fabricated *via the* hydrothermal method. For instance, the $Ti_3C_2/MoS_2/TiO_2$ composites were synthesized by the hydrothermal process in which the TiO_2 nanoparticles were assembled *in situ* in Ti_3C_2 and MoS_2 layers [31]. Other examples used a two-step hydrothermal method to fabricate $WS_2@TiO_2@Ti_3C_2$ photocatalyst and hydrothermally synthesized method to fabricate Ti_3C_2/TiO_2 decorated black phosphorous composite [31].

Another study described nanoflower-shaped TiO_2/C nanocomposite derived $Ti_3C_2(OH_xF_{1-x})_2$) was fabricated using *in situ* alcoholysis. Results enabled to show solid catalytic activity, but only for the dehydrogenation of $NaAlH_4$ applications. Nevertheless, the finding led to enlightenment of the catalytic performance of TiO_2/C nanocomposite as the best reported Ti−based catalyst for the dehydrogenation of $NaAlH_4$ by far [160]. Even though the former results were used for dehydrogenation applications, the TiO_2/C nanocomposite is expectedly applicable for NRR electrocatalyst applications concerning their excellence in catalytic activity. As only a few reports of MXenes derivation for NRR electrocatalyst applications, further studies should pave the way in these areas of interest.
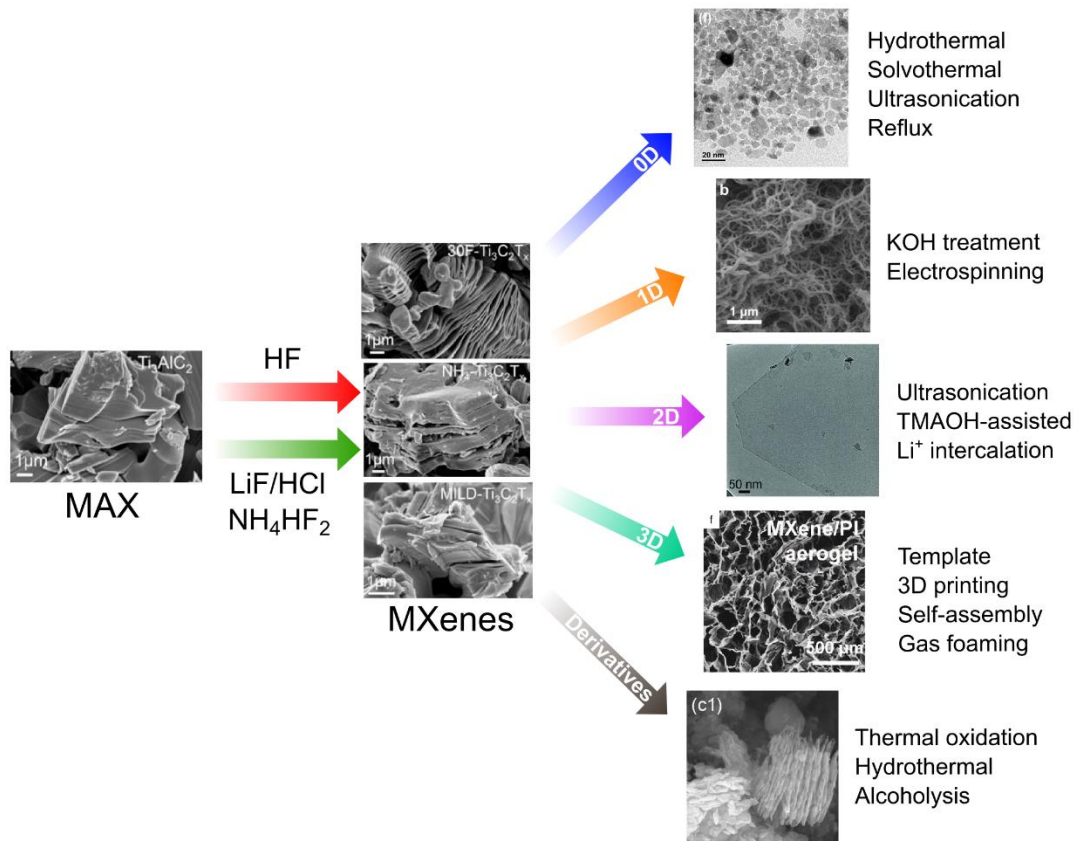
Fig. 11 Synthetic route for preparing MXenes with different structures and MXenes derivatives. Representative images are reproduced with permission from [148], [140], [135], [161], [162] and [158].

6. Conclusion, challenges, and outlook

Electrochemical and photochemical N_2 reduction reactions (NRR) have grown into attractive and alternative routes for clean ammonia (NH_3) production to the extent of significantly reducing the environmental damages impacted by the century-old and energy-intensive Haber-Bosch (HB) process. However, one massive drawback of catalytic NRR is the intrinsic competing hydrogen evolution reaction (HER) driven by the same proton (H^+) consumption. These two reactions occur at a nearly similar potential to which the latter reaction occurs as a background or metal-catalyzed process. Consequently, only a small portion of the charge is consumed to drive

the NRR, resulting in a sluggish kinetic reaction and low energy efficiency. The growing family of 2D MXenes is viewed to be more selective in aqueous solutions where the HER can be suppressed; thus, NRR can be promoted. Not only in a pristine form but MXenes can also be derived into more active catalysts and combined with other types of catalyst materials to form heterostructures. As 2D materials, MXenes could be transformed into thin-film forms, which according to our point of view, could increase the feasibility of MXenes for any devices [163], including for electro- or photo-catalyst reactors. The previous report suggested that the activity of the catalysts in the thin-film forms was improved by order of magnitude than the catalyst materials in the particulate form. Due to the maximation of specific surface area utilization of the catalyst materials in thin-film forms, it was speculated that the NH_3 production using thin-film catalyst materials would be better than catalyst materials in the particulate forms. In any case, the electrocatalysis and photocatalysis effects in the particulate form might be less pronounced than thin-film forms because the catalyst process suffers from light absorption by the catalyst particles, has light scattering rather than absorption, *etc.* [164].

Thin-film form MXenes could be possibly utilized in the industrial scale of electro- or photo-catalyst reactors because the reactor design is expected to be convenient with high recyclability and recovery, *etc.* [165]. It was speculated that the proper contact of active photocatalysts layer of a thin-film on the fixed substrate installed in the catalyst reactor could lead to efficient mass transport of reactants, intermediates, and products. On the other hand, in the case of hydrogen photocatalyst, it was predicted that the product activity values of photocatalysts in the thin-film forms are estimated to be cost-effective hydrogen production because of a low amount of material with minimum equipment. This idea is also possible to be implemented for NRR catalysts using MXenes. Furthermore, thin-film MXenes could be integrated into the reactors and thus leading to low-cost NH_3 production. However, it is still a bit premature to deduce such a firm conclusion. There are abundant tasks that need to be addressed in rationally designing the best MXenes catalyst for NRR and satisfying practical relevance. We provide a forward-looking plan on how the research direction of N_2 reduction to NH_3 over MXenes-based catalysts can be carried out, as summarized in **Fig. 12**:

(i) **Computation.** Both theoretical and experimental studies are essential to developing electro- and photo-catalyst-based MXenes. However, the gap between experimental and theoretical results

somehow resulted in new questions necessary to be answered. For instance, in catalyst research, the theoretical approach is inaccurate for predicting and understanding the molecular structure [166], and the observation by some means needs to be simplified. The theoretical method that has been simplified is also limited to studying the catalytic processes compared to the real catalysts [167]. Experimental observation is usually used to observe complete formulated catalyst systems [167] despite the combination of theoretical and experimental studies that could support each other. The interplay between experiments and theory methods should also be meaningful for studying the reactivity of those molecular structures and the kinetics of their chemical transformations [166]. To be more specific, the synergy between theoretical and experimental studies arises from kinetics observation. Here, the experimental study typically results in the phenomenological rate constants of the overall process, while computational methods contribute in disentangle them to a set of rate constants of well-defined elementary reaction steps [166]. In general, a strong correlation between them should be found to bridge the theoretical and experimental study. In this case, both studies' approaches could be conducted by simplifying the computational model system and a simplified experimental system with similar conclusions [167].

The ever-increasing computational capability in the last decades has revolutionized the field of material sciences. We are inevitably witnessing the progress of computation-aided materials discovery in predicting some promising candidates, simulating the system for a given application, and cutting a significant amount of time in experimental works. The potential of MXene as an NRR catalyst was firstly discovered by a theoretical approach using density functional theory or DFT. The discovery could interpret and analyze the practical outcomes, where many results with DFT simulation included have supported each other. Therefore, this advancement is always an exciting field to pursue. The so-called high throughput screening (HTS) can sort out the best MXenes out of hundreds of possible candidates by inputting important physical, electrical, and chemical properties for catalyzing NRR. Noting N_2 fixation under an aqueous system containing H_2O and salts electrolytes as a few examples raises more complex and dynamic reactions under different electrolytes (salts and concentration). Molecular dynamic (MD) simulation will give unforeseen insight into which NRR pathway may occur at such dynamic molecular levels to uncover the underlying mechanism of NRR in an aqueous solution. Meanwhile, machine learning and artificial intelligence can help determine actual factors predominant in NRR by looking at empirical data obtained from the experimental results.

(ii) **Structure optimization.** Even though most works of MXenes and MXenes-derived catalysts remain to focus on the $Ti_3C_2T_x$ MXene at present, theoretical studies have started seeing Mo−, Cr−, Nb−and V−based MXenes as way more promising for N_2 adsorption and activation. Thus, a progressing experimental basis requires clarifying the theoretical proposal. A recent report showed a successful synthesis of high-entropy MXenes [168]. High-entropy metal catalysts were well-known for their high mass activity to reduce CO_2 and N_2 catalytically [100–102], meaning a similar phenomenon may also occur in high-entropy MXenes. Regarding morphological design, the electrocatalytic and photocatalytic NRR process over 0D MXenes catalyst should carefully beware of their agglomeration and aggregation tendencies. Referring to that particular issue, single-atom catalysts (SACs) to enhance the NRR activity of MXenes have been promoted due to more specific surface areas for interfacial interaction between materials and molecular N_2. Therefore, MXenes and their derivatives can exhibit dual functionality as active and support materials. The use of earth-abundant metals for the synthesis of SACs is much encouraged to avoid a costly catalyst. For the heterostructures approach, however, our current understanding of the interface heterojunction formation role to the NRR properties of MXene is very limited. Moreover, the physical parameters necessitate determination to hunt the best heterostructures tandem material for MXenes, which are well-suited for practical NH_3 production with high yield and efficiency.

(iii) **Cell design.** MXenes-based catalysts have achieved the Faradaic efficiency (FE) of approximately 25% for NRR in aqueous electrolytes under ambient conditions, less than ideal for contending the conventional HB. On the other hand, the photoelectrochemical (PEC) system is seen to achieve higher energy efficiency and chemical activity for NRR since it can combine the merits of the electrocatalytic and photocatalytic processes. However, we have yet to see the use of PEC cells in N_2 reduction over MXenes-based catalysts. Lessons learned can be taken from well-established PEC water splitting as a best practice. In the PEC NRR system, the catalyst material is coated on the current collector and placed on the photocathode side, where the reduction of N_2 takes place with the help of light irradiation. The photocathode materials should possess high optical absorption to harvest solar energy. Under this context, MXenes can be combined with suitable photocatalysts semiconductors such as $BiVO_4$, g−C_3N_4, N−doped TiO_2, and many. As water oxidation occurs at the anode, one essential requirement of anode materials is to possess an excellent activity to drive oxygen-evolution reaction (OER). Noble metals (Ru, Ir, Pd, Pt) are often regarded as the best catalysts for OER, but their use should be avoided for economic concerns.

There are many exciting areas to explore within this topic alone, such as unearthing the best tandem anode materials for MXene-heterostructures-based photocathodes.

(iv) **Spectroscopy**. Although DFT can predict the NRR mechanism, it can suffer large errors originating from the exchange-correlation function that propagates into pervasive errors. It is necessary to eliminate many factors used to simplify the models, such as performing simulation in a vacuum and underestimating chemical reaction barriers. Such cases are not matched with the realistic and dynamic NRR processes as mentioned in (i). *In situ / operando* characterizations must be used to overcome the limitation of computational simulation and probe the intermediate reaction species. Nowadays, there have been many advancements in the characterization techniques applied in the catalysis field, including the catalysis of NRR [169–171]. For example, Nazemi *et al.* [172] utilized Surface-Enhanced Raman Spectroscopy (SERS) to detect the generation of NH_4^+ species upon N_2 reduction by hollow Au nanocages. Recently, *in situ* ATR mode surface-enhanced infrared absorption spectroscopy known as ATR-SEIRAS greatly benefited in uncovering the reaction intermediates and electrocatalytic NRR pathway, as Yao *et al.* [106] demonstrated. They discovered that the electrocatalytic NRR on the Au surface proceeded in the associative pathway through the formation of N_2H_y intermediates. They observed the evidence of the vibration mode of H–N–H bending, $–NH_2$ wagging, and N–N stretching in surface-bound N_2H_y species. Other examples of *in situ / operando* characterization techniques that are founded beneficial, such as a Diffusion reflection infrared Fourier transform spectroscopy (DRIFT), Shell-isolated nanoparticle-enhanced Raman spectroscopy (SHINERS), X-ray absorption fine-structure (XAFS), X-ray absorption near edge structure (XANES), paramagnetic resonance spectroscopy (EPR), etc. The *in situ / operando* spectroscopies should be employed in MXenes-based NRR catalysts to determine the active sites and reaction pathways precisely.

(v) **Economy**. NH_3 production cost *via* electrocatalytic and photocatalytic processes with the aid of MXenes-based catalysts should be lower than the HB process to be considered competitive enough. It has been estimated that the NH_3 produced by the latter method costs only US $160 per ton of NH_3, and when including the additional costs such as transportation and storage, its price increases to US $600 for the same usable quantity [173,174]. Techno-economic analysis, including SCENT (Standardized Cost Estimation for New Technology), can provide much information on whether or not the presented emerging technologies for N_2 fixation to NH_3 are economically

feasible for large- and small-scale plants. To date, the large scale of an NRR is challenging to fully compete with current HB commercial production capacities (>1000 t_{NH3}/day) considering technology readiness level. Future investigations on the integration of smaller scales with low-cost electricity sources are highly appreciated. Electricity price is the critical driver in electrocatalytic and photocatalytic NH_3 production. Since renewable energy is rapidly growing and the price is dropping accordingly, a small-scale NH_3 plant would be economically compelling and adapted to the local renewable energy sources. Therefore, it is expected to enable energy grid balance in the future energy landscape, shorten the distances corresponding to transportation and storage, and thus lower capital and operation costs. Some economic models have been developed, especially for electrochemical NRR [174,175], yet the economic feasibility for MXene-based catalysts is poorly studied. Relevant parameters to the production cost of electrochemical and photochemical systems are evaluated, and operating parameters (FE, catalysts, and current density) are optimized to meet the desired cost-effective NH_3 pricing demands.

(vi) **Environment.** With all respect to the increasing progress of MXenes catalysts for a sustainable and environmentally friendly N_2 conversion to NH_3, unfortunately, the nexus between production rate of NH_3, energy efficiency, and environmental impact has not been a focal point of many preceding experimental reports. One critical question that arises for using MXenes as NRR catalyst is, "can the energy produced from NH_3 compensate the energy input for preparing MXenes catalysts and synthesis of NH_3 itself?". Without detailed studies on environmental and energy evaluations, it is impossible to provide proper proof of a sustainable NH_3 energy landscape for MXenes. In this context, life cycle assessment (LCA) is a primary tool and international standardized method to comprehensively evaluate the environmental impact of proposed methods (both qualitatively and quantitively), considering all inputs and emissions from the NH_3 production. Using the given methodology, the produced greenhouse gases emission (in the unit of CO_2 – equivalent) as well as indirect and direct energy use throughout the life cycle from synthesis, extraction, manufacturing, production, and disposal (known as cumulative energy demand) can be compared with the existing HB process. Sustainable electrocatalytic and photocatalytic NH_3 production would only reduce environmental impacts (preferably LCA results) by coupling renewable electricity supplies with high capacity factors. This is because intermittency, seasonal, and geographic constraints are associated with the nature of renewable energy, making NH_3 production pathways utilizing renewable energy less attractive. To this extent, significant research

works should be made to realize the system integration of NH_3 production with reliable and low-cost electricity sources to compete with the current-day HB process.
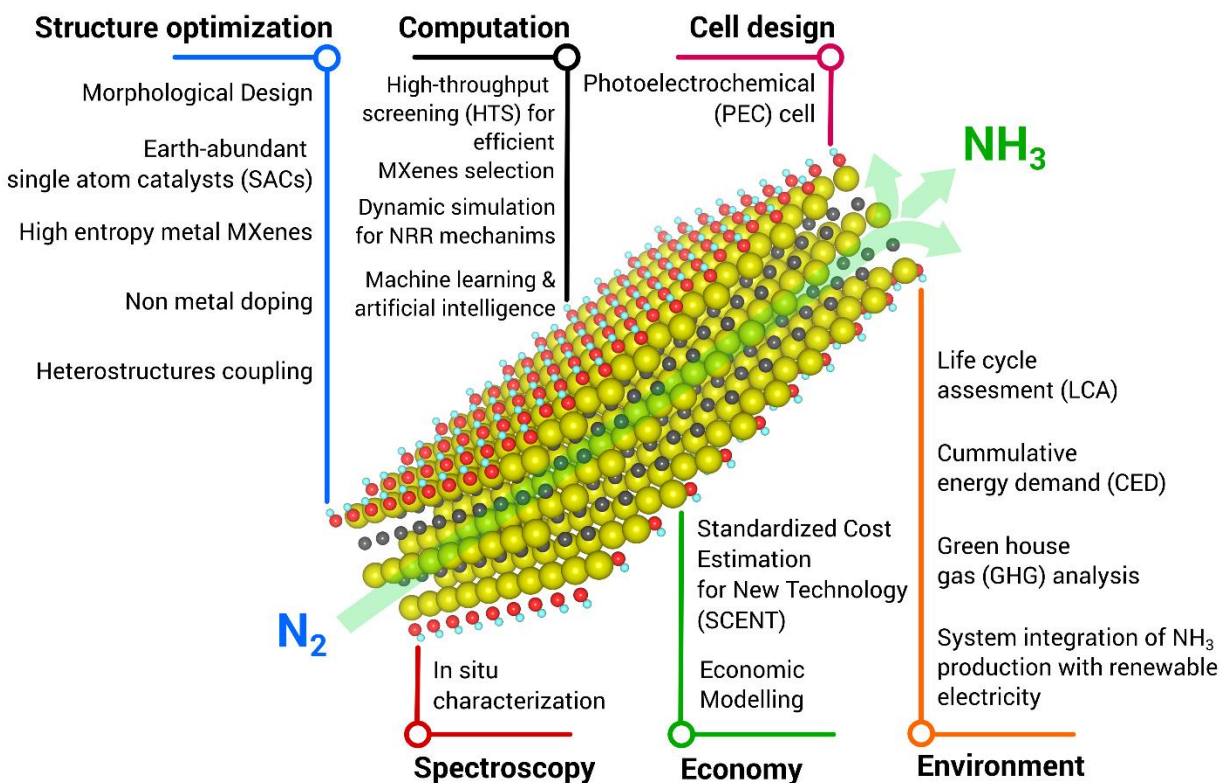

Fig. 12 Future research direction of N_2 reduction to NH_3 over MXenes and MXenes derivatives based on electrocatalyst and photocatalysts.

Author contribution

Writing - Original Draft, Investigation, Funding acquisition: **Tahta Amrillah**; Conceptualization, Methodology, Visualization, Writing - Original Draft, Writing - Review & Editing: **Angga Hermawan**; Writing - Review & Editing, Funding acquisition: **Vani Novita Alviani**; Supervision, Writing - Review & Editing, Funding acquisition: **Shu Yin & Zhi Wei Seh**. **T. Amrillah** and **A. Hermawan** are the main contributors to this manuscript.

References:

[1]   Z. Wu, R. Zhang, H. Fei, R. Liu, D. Wang, X. Liu, Multiphasic 1T@2H MoSe2 as a highly efficient catalyst for the N2 reduction to NH3, Appl. Surf. Sci. 532 (2020) 147372. doi:10.1016/j.apsusc.2020.147372.

[2]   X. Guo, H. Du, F. Qu, J. Li, Recent progress in electrocatalytic nitrogen reduction, J. Mater. Chem. A. 7 (2019) 3531–3543. doi:10.1039/C8TA11201K.

[3]   A. Good, Toward nitrogen-fixing plants, Science (80-.). 359 (2018) 869–870. doi:10.1126/science.aas8737.

[4]   Y. Song, T. Wang, J. Sun, Z. Wang, Y. Luo, L. Zhang, H. Ye, X. Sun, Enhanced Electrochemical N2 Reduction to NH3 on Reduced Graphene Oxide by Tannic Acid Modification, ACS Sustain. Chem. Eng. 7 (2019) 14368–14372. doi:10.1021/acssuschemeng.9b03890.

[5]   H. Li, S. Wei, H. Wang, Q. Cai, J. Zhao, Enhanced catalytic activity of MXene for nitrogen electoreduction reaction by carbon doping, J. Colloid Interface Sci. 588 (2021) 1–8. doi:10.1016/j.jcis.2020.12.034.

[6]   T. Shang, Z. Lin, C. Qi, X. Liu, P. Li, Y. Tao, Z. Wu, D. Li, P. Simon, Q. Yang, 3D Macroscopic Architectures from Self-Assembled MXene Hydrogels, Adv. Funct. Mater. 29 (2019) 1903960. doi:10.1002/adfm.201903960.

[7]   S.L. Foster, S.I.P. Bakovic, R.D. Duda, S. Maheshwari, R.D. Milton, S.D. Minteer, M.J. Janik, J.N. Renner, L.F. Greenlee, Catalysts for nitrogen reduction to ammonia, Nat. Catal. 1 (2018) 490–500. doi:10.1038/s41929-018-0092-7.

[8]   M. Li, H. Huang, J. Low, C. Gao, R. Long, Y. Xiong, Recent Progress on Electrocatalyst and Photocatalyst Design for Nitrogen Reduction, Small Methods. 3 (2019) 1800388. doi:10.1002/smtd.201800388.

[9]   X. Xue, R. Chen, C. Yan, P. Zhao, Y. Hu, W. Zhang, S. Yang, Z. Jin, Review on photocatalytic and electrocatalytic artificial nitrogen fixation for ammonia synthesis at mild conditions: Advances, challenges and perspectives, Nano Res. 12 (2019) 1229–1249. doi:10.1007/s12274-018-2268-5.

[10]   C. Guo, J. Ran, A. Vasileff, S.Z. Qiao, Rational design of electrocatalysts and photo(electro)catalysts for nitrogen reduction to ammonia (NH3) under ambient conditions, Energy Environ. Sci. 11 (2018) 45–56. doi:10.1039/c7ee02220d.

[11]   Z.W. She, J. Kibsgaard, C.F. Dickens, I. Chorkendorff, J.K. Nørskov, T.F. Jaramillo, Combining theory and experiment in electrocatalysis: Insights into materials design, Science (80-.). 355 (2017). doi:10.1126/science.aad4998.

[12]   Q. Wang, J. Guo, P. Chen, Recent progress towards mild-condition ammonia synthesis, J. Energy Chem. 36 (2019) 25–36. doi:10.1016/j.jechem.2019.01.027.

[13]   X. Yan, D. Liu, H. Cao, F. Hou, J. Liang, S.X. Dou, Nitrogen Reduction to Ammonia on Atomic-Scale Active Sites under Mild Conditions, Small Methods. 3 (2019) 1800501. doi:10.1002/smtd.201800501.

[14]   X. Cui, C. Tang, Q. Zhang, A Review of Electrocatalytic Reduction of Dinitrogen to Ammonia under Ambient Conditions, Adv. Energy Mater. 8 (2018) 1800369. doi:10.1002/aenm.201800369.

[15]   J. Hou, M. Yang, J. Zhang, Recent advances in catalysts, electrolytes and electrode engineering for the nitrogen reduction reaction under ambient conditions, Nanoscale. 12 (2020) 6900–6920. doi:10.1039/D0NR00412J.

[16]   J. Deng, J.A. Iñiguez, C. Liu, Electrocatalytic Nitrogen Reduction at Low Temperature, Joule. 2 (2018) 846–856. doi:10.1016/j.joule.2018.04.014.

[17]   J. John, D.-K. Lee, U. Sim, Photocatalytic and electrocatalytic approaches towards atmospheric nitrogen reduction to ammonia under ambient conditions, Nano Converg. 6 (2019) 15. doi:10.1186/s40580-019-0182-5.

[18]   Q. Chen, X. Zhang, Y. Jin, X. Zhou, Z. Yang, H. Nie, An Overview on Noble Metal (Group VIII)-based Heterogeneous Electrocatalysts for Nitrogen Reduction Reaction, Chem. - An Asian J. 15 (2020) 4131–4152. doi:10.1002/asia.202000969.

[19]   B.H.R. Suryanto, H.-L. Du, D. Wang, J. Chen, A.N. Simonov, D.R. MacFarlane, Challenges and prospects in the catalysis of electroreduction of nitrogen to ammonia, Nat. Catal. 2 (2019) 290–296. doi:10.1038/s41929-019-0252-4.

[20]   L. Shi, Y. Yin, S. Wang, H. Sun, Rational Catalyst Design for N2Reduction under Ambient Conditions: Strategies toward Enhanced Conversion Efficiency, ACS Catal. 10 (2020) 6870–6899. doi:10.1021/acscatal.0c01081.

[21]   A. Liu, X. Liang, X. Ren, W. Guan, M. Gao, Y. Yang, Q. Yang, L. Gao, Y. Li, T. Ma, Recent Progress in MXene-Based Materials: Potential High-Performance Electrocatalysts, Adv. Funct. Mater. 30 (2020) 1–22. doi:10.1002/adfm.202003437.

[22]   Y. Gogotsi, B. Anasori, The Rise of MXenes, ACS Nano. 13 (2019) 8491–8494.

doi:10.1021/acsnano.9b06394.

[23] D. Xiong, X. Li, Z. Bai, S. Lu, Recent Advances in Layered Ti3C2Tx MXene for Electrochemical Energy Storage, Small. 14 (2018) 1703419. doi:10.1002/smll.201703419.

[24] S. Sun, C. Liao, A.M. Hafez, H. Zhu, S. Wu, Two-dimensional MXenes for energy storage, Chem. Eng. J. 338 (2018) 27–45. doi:10.1016/j.cej.2017.12.155.

[25] J. Pang, R.G. Mendes, A. Bachmatiuk, L. Zhao, H.Q. Ta, T. Gemming, H. Liu, Z. Liu, M.H. Rummeli, Applications of 2D MXenes in energy conversion and storage systems, Chem. Soc. Rev. 48 (2019) 72–133. doi:10.1039/c8cs00324f.

[26] Q. Jiang, Y. Lei, H. Liang, K. Xi, C. Xia, H.N. Alshareef, Review of MXene electrochemical microsupercapacitors, Energy Storage Mater. 27 (2020) 78–95. doi:10.1016/j.ensm.2020.01.018.

[27] A. Hermawan, B. Zhang, A. Taufik, Y. Asakura, T. Hasegawa, J. Zhu, P. Shi, S. Yin, CuO Nanoparticles/Ti$_3$C$_2$T$_x$ MXene Hybrid Nanocomposites for Detection of Toluene Gas, ACS Appl. Nano Mater. 3 (2020) 4755–4766. doi:10.1021/acsanm.0c00749.

[28] Z. Wang, F. Wang, A. Hermawan, Y. Asakura, T. Hasegawa, H. Kumagai, H. Kato, M. Kakihana, J. Zhu, S. Yin, SnO-SnO2 modified two-dimensional MXene Ti3C2Tx for acetone gas sensor working at room temperature, J. Mater. Sci. Technol. 73 (2021) 128–138. doi:10.1016/j.jmst.2020.07.040.

[29] P.K. Kalambate, S.W. Zote, Y. Shen, D.N. Navale, D.K. Kulal, J. Wu, P.B. Ranade, R. Pothu, R. Boddula, Y. Huang, MXene and its Sensing Applications, in: MXenes Fundam. Appl., Materials Research Foundations, 2019: pp. 204–215. doi:10.21741/9781644900253-9.

[30] J.D. Gouveia, Á. Morales-García, F. Viñes, J.R.B. Gomes, F. Illas, Facile Heterogeneously Catalyzed Nitrogen Fixation by MXenes, ACS Catal. 10 (2020) 5049–5056. doi:10.1021/acscatal.0c00935.

[31] Q. Zhong, Y. Li, G. Zhang, Two-dimensional MXene-based and MXene-derived photocatalysts: Recent developments and perspectives, Chem. Eng. J. 409 (2021) 128099. doi:10.1016/j.cej.2020.128099.

[32] Z.W. Seh, K.D. Fredrickson, B. Anasori, J. Kibsgaard, A.L. Strickler, M.R. Lukatskaya, Y. Gogotsi, T.F. Jaramillo, A. Vojvodic, Two-Dimensional Molybdenum Carbide (MXene) as an Efficient Electrocatalyst for Hydrogen Evolution, ACS Energy Lett. 1 (2016) 589–594. doi:10.1021/acsenergylett.6b00247.

[33] K.R.G. Lim, A.D. Handoko, S.K. Nemani, B. Wyatt, H.Y. Jiang, J. Tang, B. Anasori, Z.W. Seh, Rational Design of Two-Dimensional Transition Metal Carbide/Nitride (MXene) Hybrids and Nanocomposites for Catalytic Energy Storage and Conversion, ACS Nano. 14 (2020) 10834–10864. doi:10.1021/acsnano.0c05482.

[34] A.D. Handoko, H. Chen, Y. Lum, Q. Zhang, B. Anasori, Z.W. Seh, Two-Dimensional Titanium and Molybdenum Carbide MXenes as Electrocatalysts for CO2 Reduction, IScience. 23 (2020) 101181. doi:10.1016/j.isci.2020.101181.

[35] A.D. Handoko, K.H. Khoo, T.L. Tan, H. Jin, Z.W. Seh, Establishing new scaling relations on two-dimensional MXenes for CO2 electroreduction, J. Mater. Chem. A. 6 (2018) 21885–21890. doi:10.1039/c8ta06567e.

[36] K.R.G. Lim, A.D. Handoko, L.R. Johnson, X. Meng, M. Lin, G.S. Subramanian, B. Anasori, Y. Gogotsi, A. Vojvodic, Z.W. Seh, 2H-MoS2 on Mo2CTx MXene nanohybrid for efficient and durable electrocatalytic hydrogen evolution, ACS Nano. 14 (2020) 16140–16155. doi:10.1021/acsnano.0c08671.

[37] M.M. Tunesi, R.A. Soomro, X. Han, Q. Zhu, Y. Wei, B. Xu, Application of MXenes in environmental remediation technologies, Nano Converg. 8 (2021) 5. doi:10.1186/s40580-021-00255-w.

[38] X. Feng, Z. Yu, Y. Sun, R. Long, M. Shan, X. Li, Y. Liu, J. Liu, Review MXenes as a new type of nanomaterial for environmental applications in the photocatalytic degradation of water pollutants, Ceram. Int. 47 (2021) 7321–7343. doi:10.1016/j.ceramint.2020.11.151.

[39] Y. Sun, Y. Li, Potential environmental applications of MXenes: A critical review, Chemosphere. 271 (2021) 129578. doi:10.1016/j.chemosphere.2021.129578.

[40] K. Huang, Z. Li, J. Lin, G. Han, P. Huang, Two-dimensional transition metal carbides and nitrides (MXenes) for biomedical applications, Chem. Soc. Rev. 47 (2018) 5109–5124. doi:10.1039/C7CS00838D.

[41] H. Huang, R. Jiang, Y. Feng, H. Ouyang, N. Zhou, X. Zhang, Y. Wei, Recent development and prospects of surface modification and biomedical applications of MXenes, Nanoscale. 12 (2020) 1325–1338. doi:10.1039/C9NR07616F.

[42] H. Lin, Y. Chen, J. Shi, Insights into 2D MXenes for Versatile Biomedical Applications: Current Advances and Challenges Ahead, Adv. Sci. 5 (2018) 1800518. doi:10.1002/advs.201800518.

[43] Z. Liu, H.N. Alshareef, MXenes for Optoelectronic Devices, Adv. Electron. Mater. 2100295 (2021) 2100295. doi:10.1002/aelm.202100295.

[44] Z. Liu, H.N. Alshareef, MXenes for Optoelectronic Devices, Adv. Electron. Mater. 30 (2021) 2100295. doi:10.1002/aelm.202100295.

[45] X. Zhang, J. Shao, C. Yan, R. Qin, Z. Lu, H. Geng, T. Xu, L. Ju, A review on optoelectronic device applications of 2D transition metal carbides and nitrides, Mater. Des. 200 (2021) 109452. doi:10.1016/j.matdes.2021.109452.

[46] A. Iqbal, P. Sambyal, C.M. Koo, 2D MXenes for Electromagnetic Shielding: A Review, Adv. Funct. Mater. 30 (2020) 2000883. doi:10.1002/adfm.202000883.

[47] W. Yang, J. Yang, J.J. Byun, F.P. Moissinac, J. Xu, S.J. Haigh, M. Domingos, M.A. Bissett, R.A.W. Dryfe, S. Barg, 3D Printing of Freestanding MXene Architectures for Current-Collector-Free Supercapacitors, Adv. Mater. 31 (2019) 1902725. doi:10.1002/adma.201902725.

[48] M. Khazaei, A. Ranjbar, M. Arai, T. Sasaki, S. Yunoki, Electronic properties and

applications of MXenes: a theoretical review, J. Mater. Chem. C. 5 (2017) 2488–2503. doi:10.1039/C7TC00140A.

[49] J.-C. Lei, X. Zhang, Z. Zhou, Recent advances in MXene: Preparation, properties, and applications, Front. Phys. 10 (2015) 276–286. doi:10.1007/s11467-015-0493-x.

[50] B. Anasori, M.R. Lukatskaya, Y. Gogotsi, 2D metal carbides and nitrides (MXenes) for energy storage, Nat. Rev. Mater. 2 (2017). doi:10.1038/natrevmats.2016.98.

[51] L.M. Azofra, N. Li, D.R. Macfarlane, C. Sun, Promising prospects for 2D d2-d4 M3C2 transition metal carbides (MXenes) in N2 capture and conversion into ammonia, Energy Environ. Sci. 9 (2016) 2545–2549. doi:10.1039/c6ee01800a.

[52] M. Shao, Y. Shao, W. Chen, K.L. Ao, R. Tong, Q. Zhu, I.N. Chan, W.F. Ip, X. Shi, H. Pan, Efficient nitrogen fixation to ammonia on MXenes, Phys. Chem. Chem. Phys. 20 (2018) 14504–14512. doi:10.1039/c8cp01396a.

[53] J. Zhao, L. Zhang, X.Y. Xie, X. Li, Y. Ma, Q. Liu, W.H. Fang, X. Shi, G. Cui, X. Sun, Ti3C2Tx (T = F, OH) MXene nanosheets: Conductive 2D catalysts for ambient electrohydrogenation of N2 to NH3, J. Mater. Chem. A. 6 (2018) 24031–24035. doi:10.1039/c8ta09840a.

[54] Q. Liu, L. Ai, J. Jiang, MXene-derived TiO2@C/g-C3N4 heterojunctions for highly efficient nitrogen photofixation, J. Mater. Chem. A. 6 (2018) 4102–4110. doi:10.1039/c7ta09350k.

[55] K. Huang, C. Li, H. Li, G. Ren, L. Wang, W. Wang, X. Meng, Photocatalytic applications of two-dimensional Ti3C2MXenes: A review, ACS Appl. Nano Mater. 3 (2020) 9581–9603. doi:10.1021/acsanm.0c02481.

[56] X. Li, Y. Bai, X. Shi, N. Su, G. Nie, R. Zhang, H. Nie, L. Ye, Applications of MXene (Ti 3 C 2 T x) in photocatalysis: a review , Mater. Adv. 2 (2021) 1570–1594. doi:10.1039/d0ma00938e.

[57] Z. Kang, M.A. Khan, Y. Gong, R. Javed, Y. Xu, D. Ye, H. Zhao, J. Zhang, Recent progress of MXenes and MXene-based nanomaterials for the electrocatalytic hydrogen evolution reaction, J. Mater. Chem. A. 9 (2021) 6089–6108. doi:10.1039/D0TA11735H.

[58] A.D. Handoko, S.N. Steinmann, Z.W. Seh, Theory-guided materials design: Two-dimensional MXenes in electro- and photocatalysis, Nanoscale Horizons. 4 (2019) 809–827. doi:10.1039/c9nh00100j.

[59] S. He, Q. Zhu, R.A. Soomro, B. Xu, MXene derivatives for energy storage applications, Sustain. Energy Fuels. 4 (2020) 4988–5004. doi:10.1039/d0se00927j.

[60] Y. Sun, D. Chen, Z. Liang, Two-dimensional MXenes for energy storage and conversion applications, Mater. Today Energy. 5 (2017) 22–36. doi:10.1016/j.mtener.2017.04.008.

[61] J. Sun, W. Kong, Z. Jin, Y. Han, L. Ma, X. Ding, Y. Niu, Y. Xu, Recent advances of MXene as promising catalysts for electrochemical nitrogen reduction reaction, Chinese Chem. Lett. 31 (2020) 953–960. doi:10.1016/j.cclet.2020.01.035.

[62] C.C. Leong, Y. Qu, Y. Kawazoe, S.K. Ho, H. Pan, MXenes: Novel electrocatalysts for hydrogen production and nitrogen reduction, Catal. Today. 370 (2021) 2–13. doi:10.1016/j.cattod.2020.10.003.

[63] J. Feng, H. Pan, Electronic state optimization for electrochemical N2reduction reaction in aqueous solution, J. Mater. Chem. A. 8 (2020) 13896–13915. doi:10.1039/d0ta04709k.

[64] J. Wang, C. He, J. Huo, L. Fu, C. Zhao, A Theoretical Evaluation of Possible N 2 Reduction Mechanism on Mo 2 B 2, Adv. Theory Simulations. 4 (2021) 2100003. doi:10.1002/adts.202100003.

[65] Y. Li, L. Li, R. Huang, Y. Wen, Computational screening of MBene monolayers with high electrocatalytic activity for the nitrogen reduction reaction, Nanoscale. (2021). doi:10.1039/D1NR04652G.

[66] D. Liu, M. Chen, X. Du, H. Ai, K.H. Lo, S. Wang, S. Chen, G. Xing, X. Wang, H. Pan, Development of Electrocatalysts for Efficient Nitrogen Reduction Reaction under Ambient Condition, Adv. Funct. Mater. 31 (2021) 1–36. doi:10.1002/adfm.202008983.

[67] J. Ran, J. Zhang, J. Yu, M. Jaroniec, S.Z. Qiao, Earth-abundant cocatalysts for semiconductor-based photocatalytic water splitting, Chem. Soc. Rev. 43 (2014) 7787–7812. doi:10.1039/C3CS60425J.

[68] W.J. Ong, L.L. Tan, Y.H. Ng, S.T. Yong, S.P. Chai, Graphitic Carbon Nitride (g-C3N4)-Based Photocatalysts for Artificial Photosynthesis and Environmental Remediation: Are We a Step Closer to Achieving Sustainability?, Chem. Rev. 116 (2016) 7159–7329. doi:10.1021/acs.chemrev.6b00075.

[69] Y. Gao, Y. Cao, H. Zhuo, X. Sun, Y. Gu, G. Zhuang, S. Deng, X. Zhong, Z. Wei, X. Li, J. guo Wang, Mo2TiC2 MXene: A Promising Catalyst for Electrocatalytic Ammonia Synthesis, Catal. Today. 339 (2020) 120–126. doi:10.1016/j.cattod.2018.12.029.

[70] A. Champagne, J.C. Charlier, Physical properties of 2D MXenes: From a theoretical perspective, JPhys Mater. 3 (2020). doi:10.1088/2515-7639/ab97ee.

[71] Y. Luo, G.-F. Chen, L. Ding, X. Chen, L.-X. Ding, H. Wang, Efficient Electrocatalytic N2 Fixation with MXene under Ambient Conditions, Joule. 3 (2019) 279–289. doi:10.1016/j.joule.2018.09.011.

[72] Y. Kong, D. Liu, H. Ai, K.H. Lo, S. Wang, H. Pan, Theoretical Screening of Single Atoms Supported on Two-Dimensional Nb2CN2for Nitrogen Fixation, ACS Appl. Nano Mater. 3 (2020) 11274–11281. doi:10.1021/acsanm.0c02380.

[73] Y. Luo, G.F. Chen, L. Ding, X. Chen, L.X. Ding, H. Wang, Efficient Electrocatalytic N 2 Fixation with MXene under Ambient Conditions, Joule. 3 (2019) 279–289. doi:10.1016/j.joule.2018.09.011.

[74] M. Khazaei, M. Arai, T. Sasaki, C.Y. Chung, N.S. Venkataramanan, M. Estili, Y. Sakka, Y. Kawazoe, Novel electronic and magnetic properties of two-dimensional transition metal carbides and nitrides, Adv. Funct. Mater. 23 (2013) 2185–2192. doi:10.1002/adfm.201202502.

[75] D.L. Druffel, M.G. Lanetti, J.D. Sundberg, J.T. Pawlik, M.S. Stark, C.L. Donley, L.M. McRae, K.M. Scott, S.C. Warren, Synthesis and Electronic Structure of a 3D Crystalline Stack of MXene-Like Sheets, Chem. Mater. 31 (2019) 9788–9796. doi:10.1021/acs.chemmater.9b03722.

[76] S. Shang, W. Xiong, C. Yang, B. Johannessen, R. Liu, H.-Y. Hsu, Q. Gu, M.K.H. Leung, J. Shang, Atomically Dispersed Iron Metal Site in a Porphyrin-Based Metal–Organic Framework for Photocatalytic Nitrogen Fixation, ACS Nano. 15 (2021) 9670–9678. doi:10.1021/acsnano.0c10947.

[77] D. Liu, G. Zhang, Q. Ji, Y. Zhang, J. Li, Synergistic Electrocatalytic Nitrogen Reduction Enabled by Confinement of Nanosized Au Particles onto a Two-Dimensional Ti3C2 Substrate, ACS Appl. Mater. Interfaces. 11 (2019) 25758–25765. doi:10.1021/acsami.9b02511.

[78] B. Huang, N. Li, W.J. Ong, N. Zhou, Single atom-supported MXene: How single-atomic-site catalysts tune the high activity and selectivity of electrochemical nitrogen fixation, J. Mater. Chem. A. 7 (2019) 27620–27631. doi:10.1039/c9ta09776g.

[79] Y. Fang, Z. Liu, J. Han, Z. Jin, Y. Han, F. Wang, Y. Niu, Y. Wu, Y. Xu, High-Performance Electrocatalytic Conversion of N 2 to NH 3 Using Oxygen-Vacancy-Rich TiO 2 In Situ Grown on Ti 3 C 2 T x MXene, Adv. Energy Mater. 9 (2019) 1–9. doi:10.1002/aenm.201803406.

[80] J. Qin, X. Hu, X. Li, Z. Yin, B. Liu, K. ho Lam, 0D/2D AgInS 2 /MXene Z-scheme heterojunction nanosheets for improved ammonia photosynthesis of N 2, Nano Energy. 61 (2019) 27–35. doi:10.1016/j.nanoen.2019.04.028.

[81] J. Zhao, L. Zhang, X.Y. Xie, X. Li, Y. Ma, Q. Liu, W.H. Fang, X. Shi, G. Cui, X. Sun, $Ti_3C_2T_x$ (T = F, OH) MXene nanosheets: Conductive 2D catalysts for ambient electrohydrogenation of N_2 to NH_3, J. Mater. Chem. A. 6 (2018) 24031–24035. doi:10.1039/c8ta09840a.

[82] J. Xia, H. Guo, G. Yu, Q. Chen, Y. Liu, Q. Liu, Y. Luo, T. Li, E. Traversa, 2D Vanadium Carbide (MXene) for Electrochemical Synthesis of Ammonia Under Ambient Conditions, Catal. Letters. (2021). doi:10.1007/s10562-021-03589-6.

[83] G. Yu, H. Guo, S. Liu, L. Chen, A.A. Alshehri, K.A. Alzahrani, F. Hao, T. Li, Cr3C2 Nanoparticle-Embedded Carbon Nanofiber for Artificial Synthesis of NH3 through N2 Fixation under Ambient Conditions, ACS Appl. Mater. Interfaces. 11 (2019) 35764–35769. doi:10.1021/acsami.9b12675.

[84] H. Wei, Q. Jiang, C. Ampelli, S. Chen, S. Perathoner, Y. Liu, G. Centi, Enhancing N2 Fixation Activity by Converting Ti3C2 MXenes Nanosheets to Nanoribbons, ChemSusChem. 13 (2020) 5614–5619. doi:10.1002/cssc.202001719.

[85] L. Yu, J. Qin, W. Zhao, Z. Zhang, J. Ke, B. Liu, Advances in Two-Dimensional MXenes for Nitrogen Electrocatalytic Reduction to Ammonia, Int. J. Photoenergy. 2020 (2020) 1–11. doi:10.1155/2020/5251431.

[86] Z. Jin, C. Liu, Z. Liu, J. Han, Y. Fang, Y. Han, Y. Niu, Y. Wu, C. Sun, Y. Xu, Rational

Design of Hydroxyl-Rich Ti 3 C 2 T x MXene Quantum Dots for High-Performance Electrochemical N 2 Reduction, Adv. Energy Mater. 10 (2020) 2000797. doi:10.1002/aenm.202000797.

[87] M. Velický, P.S. Toth, From two-dimensional materials to their heterostructures: An electrochemist's perspective, Appl. Mater. Today. 8 (2017) 68–103. doi:10.1016/j.apmt.2017.05.003.

[88] L. Britnell, R.M. Ribeiro, A. Eckmann, R. Jalil, B.D. Belle, A. Mishchenko, Y.-J. Kim, R. V. Gorbachev, T. Georgiou, S. V. Morozov, A.N. Grigorenko, A.K. Geim, C. Casiraghi, A.H.C. Neto, K.S. Novoselov, Strong Light-Matter Interactions in Heterostructures of Atomically Thin Films, Science (80-.). 340 (2013) 1311–1314. doi:10.1126/science.1235547.

[89] S.J. Haigh, A. Gholinia, R. Jalil, S. Romani, L. Britnell, D.C. Elias, K.S. Novoselov, L.A. Ponomarenko, A.K. Geim, R. Gorbachev, Cross-sectional imaging of individual layers and buried interfaces of graphene-based heterostructures and superlattices, Nat. Mater. 11 (2012) 764–767. doi:10.1038/nmat3386.

[90] V. Guerra, T. McNally, Surface Cleaning of 2D Materials: Boron Nitride Nanosheets (BNNS) and Exfoliated Graphite Nanoplatelets (GNP), Adv. Mater. Interfaces. 7 (2020) 1–9. doi:10.1002/admi.202000944.

[91] L.R. Johnson, S. Sridhar, L. Zhang, K.D. Fredrickson, A.S. Raman, J. Jang, C. Leach, A. Padmanabhan, C.C. Price, N.C. Frey, A. Raizada, V. Rajaraman, S.A. Saiprasad, X. Tang, A. Vojvodic, MXene Materials for the Electrochemical Nitrogen Reduction-Functionalized or Not?, ACS Catal. 10 (2020) 253–264. doi:10.1021/acscatal.9b01925.

[92] J. Xia, S.Z. Yang, B. Wang, P. Wu, I. Popovs, H. Li, S. Irle, S. Dai, H. Zhu, Boosting electrosynthesis of ammonia on surface-engineered MXene Ti3C2, Nano Energy. 72 (2020) 104681. doi:10.1016/j.nanoen.2020.104681.

[93] T. Li, X. Yan, L. Huang, J. Li, L. Yao, Q. Zhu, W. Wang, W. Abbas, R. Naz, J. Gu, Q. Liu, W. Zhang, D. Zhang, Fluorine-free Ti3C2T: X (T = O, OH) nanosheets (~50-100 nm) for nitrogen fixation under ambient conditions, J. Mater. Chem. A. 7 (2019) 14462–14465. doi:10.1039/c9ta03254a.

[94] Y. Ding, J. Zhang, A. Guan, Q. Wang, S. Li, A.M. Al-Enizi, L. Qian, L. Zhang, G. Zheng, Promoting N2 electroreduction to ammonia by fluorine-terminating Ti3C2Tx MXene, Nano Converg. 8 (2021) 14. doi:10.1186/s40580-021-00264-9.

[95] S. Zheng, S. Li, Z. Mei, Z. Hu, M. Chu, J. Liu, X. Chen, F. Pan, Electrochemical Nitrogen Reduction Reaction Performance of Single-Boron Catalysts Tuned by MXene Substrates, J. Phys. Chem. Lett. 10 (2019) 6984–6989. doi:10.1021/acs.jpclett.9b02741.

[96] Y. Guo, T. Wang, Q. Yang, X. Li, H. Li, Y. Wang, T. Jiao, Z. Huang, B. Dong, W. Zhang, J. Fan, C. Zhi, Highly Efficient Electrochemical Reduction of Nitrogen to Ammonia on Surface Termination Modified Ti3C2TxMXene Nanosheets, ACS Nano. 14 (2020) 9089–9097. doi:10.1021/acsnano.0c04284.

[97] A. Liu, X. Liang, Q. Yang, X. Ren, M. Gao, Y. Yang, T. Ma, Electrocatalytic Synthesis of

Ammonia Using a 2D Ti3C2 MXene Loaded with Copper Nanoparticles, Chempluschem. 86 (2021) 166–170. doi:10.1002/cplu.202000702.

[98] C.F. Du, L. Yang, K. Tang, W. Fang, X. Zhao, Q. Liang, X. Liu, H. Yu, W. Qi, Q. Yan, Ni nanoparticles/V4C3TxMXene heterostructures for electrocatalytic nitrogen fixation, Mater. Chem. Front. 5 (2021) 2338–2346. doi:10.1039/d0qm00898b.

[99] W. Peng, M. Luo, X. Xu, K. Jiang, M. Peng, D. Chen, T. Chan, Y. Tan, Spontaneous Atomic Ruthenium Doping in Mo 2 CT X MXene Defects Enhances Electrocatalytic Activity for the Nitrogen Reduction Reaction, Adv. Energy Mater. 10 (2020) 2001364. doi:10.1002/aenm.202001364.

[100] A. Liu, M. Gao, X. Ren, F. Meng, Y. Yang, Q. Yang, W. Guan, L. Gao, X. Liang, T. Ma, A two-dimensional Ru@MXene catalyst for highly selective ambient electrocatalytic nitrogen reduction, Nanoscale. 12 (2020) 10933–10938. doi:10.1039/d0nr00788a.

[101] A. Liu, Q. Yang, X. Ren, M. Gao, Y. Yang, L. Gao, Y. Li, Y. Zhao, X. Liang, T. Ma, Two-dimensional CuAg/Ti3C2catalyst for electrochemical synthesis of ammonia under ambient conditions: a combined experimental and theoretical study, Sustain. Energy Fuels. 4 (2020) 5061–5071. doi:10.1039/d0se00915f.

[102] X. Liang, X. Ren, Q. Yang, L. Gao, M. Gao, Y. Yang, H. Zhu, G. Li, T. Ma, A. Liu, A two-dimensional MXene-supported metal-organic framework for highly selective ambient electrocatalytic nitrogen reduction, Nanoscale. 13 (2021) 2843–2848. doi:10.1039/d0nr08744k.

[103] Y. Gao, H. Zhuo, Y. Cao, X. Sun, G. Zhuang, S. Deng, X. Zhong, Z. Wei, J. Wang, A theoretical study of electrocatalytic ammonia synthesis on single metal atom/MXene, Cuihua Xuebao/Chinese J. Catal. 40 (2019) 152–159. doi:10.1016/S1872-2067(18)63197-3.

[104] F. Li, H. Ai, C. Shi, K.H. Lo, H. Pan, Single transition metal atom catalysts on Ti2CN2 for efficient CO2 reduction reaction, Int. J. Hydrogen Energy. 46 (2021) 12886–12896. doi:10.1016/j.ijhydene.2021.01.096.

[105] Y. Zeng, X. Du, Y. Li, Y. Guo, Y. Xie, J. Huang, G. Rao, T. Lei, C. Gong, X. Wang, B. Sun, Synergistic performance of nitrogen and sulfur co-doped Ti3C2TX for electrohydrogenation of N2 to NH3, J. Alloys Compd. 869 (2021) 159335. doi:10.1016/j.jallcom.2021.159335.

[106] W. Kong, F. Gong, Q. Zhou, G. Yu, L. Ji, X. Sun, A.M. Asiri, T. Wang, Y. Luo, Y. Xu, An MnO2-Ti3C2T: X MXene nanohybrid: An efficient and durable electrocatalyst toward artificial N2 fixation to NH3 under ambient conditions, J. Mater. Chem. A. 7 (2019) 18823–18827. doi:10.1039/c9ta04902a.

[107] X. Xu, B. Sun, Z. Liang, H. Cui, J. Tian, High-Performance Electrocatalytic Conversion of N2to NH3Using 1T-MoS2Anchored on Ti3C2MXene under Ambient Conditions, ACS Appl. Mater. Interfaces. 12 (2020) 26060–26067. doi:10.1021/acsami.0c06744.

[108] Y. Kong, T. He, A.R. Puente Santiago, D. Liu, A. Du, S. Wang, H. Pan, Unravelling the Reaction Mechanisms of N2 Fixation on Molybdenum Nitride: A Full DFT Study from

the Pristine Surface to Heteroatom Anchoring, ChemSusChem. 14 (2021) 3257–3266. doi:10.1002/cssc.202101014.

[109] Z. Ma, J. Chen, D. Luo, T. Thersleff, R. Dronskowski, A. Slabon, Structural evolution of CrN nanocube electrocatalysts during nitrogen reduction reaction, Nanoscale. 12 (2020) 19276–19283. doi:10.1039/d0nr04981f.

[110] X. Zhang, R.M. Kong, H. Du, L. Xia, F. Qu, Highly efficient electrochemical ammonia synthesis: Via nitrogen reduction reactions on a VN nanowire array under ambient conditions, Chem. Commun. 54 (2018) 5323–5325. doi:10.1039/c8cc00459e.

[111] J. Zhang, L. Yang, H. Wang, G. Zhu, H. Wen, H. Feng, X. Sun, X. Guan, J. Wen, Y. Yao, In Situ Hydrothermal Growth of TiO 2 Nanoparticles on a Conductive Ti 3 C 2 T x MXene Nanosheet: A Synergistically Active Ti-Based Nanohybrid Electrocatalyst for Enhanced N 2 Reduction to NH 3 at Ambient Conditions, Inorg. Chem. 58 (2019) 5414–5418. doi:10.1021/acs.inorgchem.9b00606.

[112] B. Sun, P. Qiu, Z. Liang, Y. Xue, X. Zhang, L. Yang, H. Cui, J. Tian, The fabrication of 1D/2D CdS nanorod@Ti3C2 MXene composites for good photocatalytic activity of hydrogen generation and ammonia synthesis, Chem. Eng. J. 406 (2021) 127177. doi:10.1016/j.cej.2020.127177.

[113] J. Qin, B. Liu, K.H. Lam, S. Song, X. Li, X. Hu, 0D/2D MXene Quantum Dot/Ni-MOF Ultrathin Nanosheets for Enhanced N2Photoreduction, ACS Sustain. Chem. Eng. 8 (2020) 17791–17799. doi:10.1021/acssuschemeng.0c06388.

[114] Y. Liao, J. Qian, G. Xie, Q. Han, W. Dang, Y. Wang, L. Lv, S. Zhao, L. Luo, W. Zhang, H.-Y. Jiang, J. Tang, 2D-layered Ti3C2 MXenes for promoted synthesis of NH3 on P25 photocatalysts, Appl. Catal. B Environ. 273 (2020) 119054. doi:10.1016/j.apcatb.2020.119054.

[115] C. Sun, Z. Chen, J. Cui, K. Li, H. Qu, H. Xie, Q. Zhong, Site-exposed Ti3C2MXene anchored in N-defect g-C3N4heterostructure nanosheets for efficient photocatalytic N2fixation, Catal. Sci. Technol. 11 (2021) 1027–1038. doi:10.1039/d0cy01955k.

[116] C. Hao, Y. Liao, Y. Wu, Y. An, J. Lin, Z. Gu, M. Jiang, S. Hu, X. Wang, RuO2-loaded TiO2–MXene as a high performance photocatalyst for nitrogen fixation, J. Phys. Chem. Solids. 136 (2020) 109141. doi:10.1016/j.jpcs.2019.109141.

[117] T. Hou, Q. Li, Y. Zhang, W. Zhu, K. Yu, S. Wang, Q. Xu, S. Liang, L. Wang, Near-infrared light-driven photofixation of nitrogen over Ti3C2Tx/TiO2 hybrid structures with superior activity and stability, Appl. Catal. B Environ. 273 (2020) 119072. doi:10.1016/j.apcatb.2020.119072.

[118] W. Gao, X. Li, S. Luo, Z. Luo, X. Zhang, R. Huang, M. Luo, In situ modification of cobalt on MXene/TiO2 as composite photocatalyst for efficient nitrogen fixation, J. Colloid Interface Sci. 585 (2021) 20–29. doi:10.1016/j.jcis.2020.11.064.

[119] M. Sokol, V. Natu, S. Kota, M.W. Barsoum, On the Chemical Diversity of the MAX Phases, Trends Chem. 1 (2019) 210–223. doi:10.1016/j.trechm.2019.02.016.

[120] G. Zhao, X. Wang, C. Xu, MXene-Derived Nanocomposites as Earth-Abundant Efficient

Electrocatalyst for Nitrogen Reduction Reaction under Ambient Conditions, Inorg. Chem. 59 (2020) 16672–16678. doi:10.1021/acs.inorgchem.0c02671.

[121] J. Qian, S. Zhao, W. Dang, Y. Liao, W. Zhang, H. Wang, L. Lv, L. Luo, H. Jiang, J. Tang, Photocatalytic Nitrogen Reduction by Ti 3 C 2 MXene Derived Oxygen Vacancy-Rich C/TiO 2, Adv. Sustain. Syst. 5 (2021) 2000282. doi:10.1002/adsu.202000282.

[122] S. Wang, B. Li, L. Li, Z. Tian, Q. Zhang, L. Chen, X.C. Zeng, Highly efficient N2 fixation catalysts: Transition-metal carbides M2C (MXenes), Nanoscale. 12 (2020) 538–547. doi:10.1039/c9nr09157b.

[123] Y. Tian, Y. An, H. Wei, C. Wei, Y. Tao, Y. Li, B. Xi, S. Xiong, J. Feng, Y. Qian, Micron-Sized Nanoporous Vanadium Pentoxide Arrays for High-Performance Gel Zinc-Ion Batteries and Potassium Batteries, Chem. Mater. 32 (2020) 4054–4064. doi:10.1021/acs.chemmater.0c00787.

[124] J. Han, X. Ji, X. Ren, G. Cui, L. Li, F. Xie, H. Wang, B. Li, X. Sun, MoO 3 nanosheets for efficient electrocatalytic N 2 fixation to NH 3, J. Mater. Chem. A. 6 (2018) 12974–12977. doi:10.1039/C8TA03974G.

[125] J. Wang, Y.P. Liu, H. Zhang, D.J. Huang, K. Chu, Ambient electrocatalytic nitrogen reduction on a MoO2/graphene hybrid: Experimental and DFT studies, Catal. Sci. Technol. 9 (2019) 4248–4254. doi:10.1039/c9cy00907h.

[126] H. Jiang, C. Zang, Y. Zhang, W. Wang, C. Yang, B. Sun, Y. Shen, F. Bian, 2D MXene-derived Nb2O5/C/Nb2C/g-C3N4heterojunctions for efficient nitrogen photofixation, Catal. Sci. Technol. 10 (2020) 5964–5972. doi:10.1039/d0cy00656d.

[127] J. Liu, W. Peng, Y. Li, F. Zhang, X. Fan, 2D MXene-Based Materials for Electrocatalysis, Trans. Tianjin Univ. 26 (2020) 149–171. doi:10.1007/s12209-020-00235-x.

[128] H. Huang, Y. Song, N. Li, D. Chen, Q. Xu, H. Li, J. He, J. Lu, One-step in-situ preparation of N-doped TiO2@C derived from Ti3C2 MXene for enhanced visible-light driven photodegradation, Appl. Catal. B Environ. 251 (2019) 154–161. doi:10.1016/j.apcatb.2019.03.066.

[129] X. Xie, N. Zhang, Positioning MXenes in the Photocatalysis Landscape: Competitiveness, Challenges, and Future Perspectives, Adv. Funct. Mater. 30 (2020) 1–23. doi:10.1002/adfm.202002528.

[130] S.A. Khan, B. Amin, L.Y. Gan, I. Ahmad, Strain engineering of electronic structures and photocatalytic responses of MXenes functionalized by oxygen, Phys. Chem. Chem. Phys. 19 (2017) 14738–14744. doi:10.1039/c7cp02513k.

[131] J. Cui, Q. Peng, J. Zhou, Z. Sun, Strain-tunable electronic structures and optical properties of semiconducting MXenes, Nanotechnology. 30 (2019). doi:10.1088/1361-6528/ab1f22.

[132] Z. Guo, N. Miao, J. Zhou, B. Sa, Z. Sun, Strain-mediated type-I/type-II transition in MXene/Blue phosphorene van der Waals heterostructures for flexible optical/electronic devices, J. Mater. Chem. C. 5 (2017) 978–984. doi:10.1039/c6tc04349f.

[133] L. Tian, Z. Li, P. Wang, X. Zhai, X. Wang, T. Li, Carbon quantum dots for advanced

electrocatalysis, J. Energy Chem. 55 (2021) 279–294. doi:10.1016/j.jechem.2020.06.057.

[134] Q. Xue, H. Zhang, M. Zhu, Z. Pei, H. Li, Z. Wang, Y. Huang, Y. Huang, Q. Deng, J. Zhou, S. Du, Q. Huang, C. Zhi, Photoluminescent Ti3C2 MXene Quantum Dots for Multicolor Cellular Imaging, Adv. Mater. 29 (2017). doi:10.1002/adma.201604847.

[135] S. Lu, L. Sui, Y. Liu, X. Yong, G. Xiao, K. Yuan, Z. Liu, B. Liu, B. Zou, B. Yang, White Photoluminescent Ti 3 C 2 MXene Quantum Dots with Two-Photon Fluorescence, Adv. Sci. 6 (2019) 1801470. doi:10.1002/advs.201801470.

[136] Y. Qin, Z. Wang, N. Liu, Y. Sun, D. Han, Y. Liu, L. Niu, Z. Kang, High-yield fabrication of Ti3C2Tx MXene quantum dots and their electrochemiluminescence behavior, Nanoscale. 10 (2018) 14000–14004. doi:10.1039/c8nr03903h.

[137] F. He, B. Zhu, B. Cheng, J. Yu, W. Ho, W. Macyk, 2D/2D/0D TiO2/C3N4/Ti3C2 MXene composite S-scheme photocatalyst with enhanced CO2 reduction activity, Appl. Catal. B Environ. 272 (2020) 119006. doi:10.1016/j.apcatb.2020.119006.

[138] Y. Li, L. Ding, Y. Guo, Z. Liang, H. Cui, J. Tian, Boosting the Photocatalytic Ability of g-C3N4 for Hydrogen Production by Ti3C2 MXene Quantum Dots, ACS Appl. Mater. Interfaces. 11 (2019) 41440–41447. doi:10.1021/acsami.9b14985.

[139] Z. Zeng, Y. Yan, J. Chen, P. Zan, Q. Tian, P. Chen, Boosting the Photocatalytic Ability of Cu2O Nanowires for CO2 Conversion by MXene Quantum Dots, Adv. Funct. Mater. 29 (2019). doi:10.1002/adfm.201806500.

[140] P. Lian, Y. Dong, Z.S. Wu, S. Zheng, S. Wang, C. Sun, J. Qin, X. Shi, X. Bao, Alkalized Ti3C2 MXene nanoribbons with expanded interlayer spacing for high-capacity sodium and potassium ion batteries, Nano Energy. 40 (2017) 1–8. doi:10.1016/j.nanoen.2017.08.002.

[141] W. Yuan, L. Cheng, Y. An, H. Wu, N. Yao, X. Fan, X. Guo, MXene Nanofibers as Highly Active Catalysts for Hydrogen Evolution Reaction, ACS Sustain. Chem. Eng. 6 (2018) 8976–8982. doi:10.1021/acssuschemeng.8b01348.

[142] N. Li, Y. Jiang, C. Zhou, Y. Xiao, B. Meng, Z. Wang, D. Huang, C. Xing, Z. Peng, High-Performance Humidity Sensor Based on Urchin-Like Composite of Ti3C2 MXene-Derived TiO2 Nanowires, ACS Appl. Mater. Interfaces. 11 (2019) 38116–38125. doi:10.1021/acsami.9b12168.

[143] J. Huang, R. Meng, L. Zu, Z. Wang, N. Feng, Z. Yang, Y. Yu, J. Yang, Sandwich-like Na0.23TiO2 nanobelt/Ti3C2 MXene composites from a scalable in situ transformation reaction for long-life high-rate lithium/sodium-ion batteries, Nano Energy. 46 (2018) 20–28. doi:10.1016/j.nanoen.2018.01.030.

[144] X. Sun, K. Tan, Y. Liu, J. Zhang, L. Hou, C. Yuan, In-situ growth of hybrid NaTi8O13/NaTiO2 nanoribbons on layered MXene Ti3C2 as a competitive anode for high-performance sodium-ion batteries, Chinese Chem. Lett. 31 (2020) 2254–2258. doi:10.1016/j.cclet.2020.02.016.

[145] J. Timoshenko, B. Roldan Cuenya, In Situ / Operando Electrocatalyst Characterization by X-ray Absorption Spectroscopy, Chem. Rev. 121 (2021) 882–961.

doi:10.1021/acs.chemrev.0c00396.

[146] M. Tao, G. Du, T. Yang, W. Gao, L. Zhang, W. Du, J. Jiang, S. Bao, M. Xu, MXene-derived three-dimensional carbon nanotube network encapsulate CoS2 nanoparticles as an anode material for solid-state sodium-ion batteries, J. Mater. Chem. A. 8 (2020) 3018–3026. doi:10.1039/c9ta12834d.

[147] M. Xin, J. Li, Z. Ma, L. Pan, Y. Shi, MXenes and Their Applications in Wearable Sensors, Front. Chem. 8 (2020) 1–14. doi:10.3389/fchem.2020.00297.

[148] M. Alhabeb, K. Maleski, B. Anasori, P. Lelyukh, L. Clark, S. Sin, Y. Gogotsi, Guidelines for Synthesis and Processing of Two-Dimensional Titanium Carbide (Ti3C2Tx MXene), Chem. Mater. 29 (2017) 7633–7644. doi:10.1021/acs.chemmater.7b02847.

[149] L. Zhao, B. Dong, S. Li, L. Zhou, L. Lai, Z. Wang, S. Zhao, M. Han, K. Gao, M. Lu, X. Xie, B. Chen, Z. Liu, X. Wang, H. Zhang, H. Li, J. Liu, H. Zhang, X. Huang, W. Huang, Interdiffusion Reaction-Assisted Hybridization of Two-Dimensional Metal-Organic Frameworks and Ti3C2Tx Nanosheets for Electrocatalytic Oxygen Evolution, ACS Nano. 11 (2017) 5800–5807. doi:10.1021/acsnano.7b01409.

[150] S. Cao, B. Shen, T. Tong, J. Fu, J. Yu, 2D/2D Heterojunction of Ultrathin MXene/Bi 2 WO 6 Nanosheets for Improved Photocatalytic CO 2 Reduction, Adv. Funct. Mater. 28 (2018) 1800136. doi:10.1002/adfm.201800136.

[151] T. Shang, Z. Lin, C. Qi, X. Liu, P. Li, Y. Tao, Z. Wu, D. Li, P. Simon, Q. Yang, 3D Macroscopic Architectures from Self-Assembled MXene Hydrogels, Adv. Funct. Mater. 29 (2019) 1903960. doi:10.1002/adfm.201903960.

[152] P. Zhang, R.A. Soomro, Z. Guan, N. Sun, B. Xu, 3D carbon-coated MXene architectures with high and ultrafast lithium/sodium-ion storage, Energy Storage Mater. 29 (2020) 163–171. doi:10.1016/j.ensm.2020.04.016.

[153] W. Yuan, K. Yang, H. Peng, F. Li, F. Yin, A flexible VOCs sensor based on a 3D Mxene framework with a high sensing performance, J. Mater. Chem. A. 6 (2018) 18116–18124. doi:10.1039/c8ta06928j.

[154] Y. Liu, Y. He, E. Vargun, T. Plachy, P. Saha, Q. Cheng, 3D Porous Ti3C2 MXene/NiCo-MOF Composites for Enhanced Lithium Storage, Nanomaterials. 10 (2020) 695. doi:10.3390/nano10040695.

[155] H. Tang, S. Zhuang, Z. Bao, C. Lao, Y. Mei, Two-Step Oxidation of Mxene in the Synthesis of Layer-Stacked Anatase Titania with Enhanced Lithium-Storage Performance, ChemElectroChem. 3 (2016) 871–876. doi:10.1002/celc.201600078.

[156] R. Wang, S. Wang, Y. Zhang, D. Jin, X. Tao, L. Zhang, Graphene-coupled Ti3C2 MXenes-derived TiO2 mesostructure: Promising sodium-ion capacitor anode with fast ion storage and long-term cycling, J. Mater. Chem. A. 6 (2018) 1017–1027. doi:10.1039/c7ta09153b.

[157] Y. Dong, Z.S. Wu, S. Zheng, X. Wang, J. Qin, S. Wang, X. Shi, X. Bao, Ti3C2 MXene-Derived Sodium/Potassium Titanate Nanoribbons for High-Performance Sodium/Potassium Ion Batteries with Enhanced Capacities, ACS Nano. 11 (2017) 4792–

4800. doi:10.1021/acsnano.7b01165.

[158] W. Yuan, L. Cheng, Y. Zhang, H. Wu, S. Lv, L. Chai, X. Guo, L. Zheng, 2D-Layered Carbon/TiO 2 Hybrids Derived from Ti 3 C 2 MXenes for Photocatalytic Hydrogen Evolution under Visible Light Irradiation, Adv. Mater. Interfaces. 4 (2017) 1700577. doi:10.1002/admi.201700577.

[159] C. Ling, X. Niu, Q. Li, A. Du, J. Wang, Metal-Free Single Atom Catalyst for N 2 Fixation Driven by Visible Light, J. Am. Chem. Soc. 140 (2018) 14161–14168. doi:10.1021/jacs.8b07472.

[160] G. Zou, B. Liu, J. Guo, Q. Zhang, C. Fernandez, Q. Peng, Synthesis of Nanoflower-Shaped MXene Derivative with Unexpected Catalytic Activity for Dehydrogenation of Sodium Alanates, ACS Appl. Mater. Interfaces. 9 (2017) 7611–7618. doi:10.1021/acsami.6b13973.

[161] A. Lipatov, M. Alhabeb, M.R. Lukatskaya, A. Boson, Y. Gogotsi, A. Sinitskii, Effect of Synthesis on Quality, Electronic Properties and Environmental Stability of Individual Monolayer Ti 3 C 2 MXene Flakes, Adv. Electron. Mater. 2 (2016) 1600255. doi:10.1002/aelm.201600255.

[162] K. Li, M. Liang, H. Wang, X. Wang, Y. Huang, J. Coelho, S. Pinilla, Y. Zhang, F. Qi, V. Nicolosi, Y. Xu, 3D MXene Architectures for Efficient Energy Storage and Conversion, Adv. Funct. Mater. 30 (2020) 2000842. doi:10.1002/adfm.202000842.

[163] A. Hermawan, T. Amrillah, A. Riapanitra, W.J. Ong, S. Yin, Prospects and Challenges of MXenes as Emerging Sensing Materials for Flexible and Wearable Breath-Based Biomarker Diagnosis, Adv. Healthc. Mater. 2100970 (2021) 1–27. doi:10.1002/adhm.202100970.

[164] N. Nalajala, K.K. Patra, P.A. Bharad, C.S. Gopinath, Why the thin film form of a photocatalyst is better than the particulate form for direct solar-to-hydrogen conversion: A poor man's approach, RSC Adv. 9 (2019) 6094–6100. doi:10.1039/c8ra09982k.

[165] F. Khodadadian, F.G. de la Garza, J.R. van Ommen, A.I. Stankiewicz, R. Lakerveld, The application of automated feedback and feedforward control to a LED-based photocatalytic reactor, Chem. Eng. J. 362 (2019) 375–382. doi:10.1016/j.cej.2018.12.134.

[166] C. Greco, V. Fourmond, C. Baffert, P.H. Wang, S. Dementin, P. Bertrand, M. Bruschi, J. Blumberger, L. De Gioia, C. Léger, Combining experimental and theoretical methods to learn about the reactivity of gas-processing metalloenzymes, Energy Environ. Sci. 7 (2014) 3543–3573. doi:10.1039/c4ee01848f.

[167] C.K. Narula, L.F. Allard, D.A. Blom, M. Moses-Debusk, Bridging the gap between theory and experiments - nano-structural changes in supported catalysts under operating conditions, SAE Int. J. Mater. Manuf. 1 (2009) 182–188. doi:10.4271/2008-01-0416.

[168] S.K. Nemani, B. Zhang, B.C. Wyatt, Z.D. Hood, S. Manna, R. Khaledialidusti, W. Hong, M.G. Sternberg, S.K.R.S. Sankaranarayanan, B. Anasori, High-Entropy 2D Carbide MXenes: TiVNbMoC 3 and TiVCrMoC 3, ACS Nano. (2021) acsnano.1c02775. doi:10.1021/acsnano.1c02775.

[169] J. Timoshenko, B. Roldan Cuenya, In Situ/ Operando Electrocatalyst Characterization by X-ray Absorption Spectroscopy, Chem. Rev. 121 (2021) 882–961. doi:10.1021/acs.chemrev.0c00396.

[170] S. Liu, M. Wang, T. Qian, H. Ji, J. Liu, C. Yan, Facilitating nitrogen accessibility to boron-rich covalent organic frameworks via electrochemical excitation for efficient nitrogen fixation, Nat. Commun. 10 (2019) 3898. doi:10.1038/s41467-019-11846-x.

[171] A.D. Handoko, F. Wei, Jenndy, B.S. Yeo, Z.W. Seh, Understanding heterogeneous electrocatalytic carbon dioxide reduction through operando techniques, Nat. Catal. 1 (2018) 922–934. doi:10.1038/s41929-018-0182-6.

[172] M. Nazemi, S.R. Panikkanvalappil, M.A. El-Sayed, Enhancing the rate of electrochemical nitrogen reduction reaction for ammonia synthesis under ambient conditions using hollow gold nanocages, Nano Energy. 49 (2018) 316–323. doi:10.1016/j.nanoen.2018.04.039.

[173] B.M. Comer, P. Fuentes, C.O. Dimkpa, Y.H. Liu, C.A. Fernandez, P. Arora, M. Realff, U. Singh, M.C. Hatzell, A.J. Medford, Prospects and Challenges for Solar Fertilizers, Joule. 3 (2019) 1578–1605. doi:10.1016/j.joule.2019.05.001.

[174] G. Hochman, A.S. Goldman, F.A. Felder, J.M. Mayer, A.J.M. Miller, P.L. Holland, L.A. Goldman, P. Manocha, Z. Song, S. Aleti, Potential Economic Feasibility of Direct Electrochemical Nitrogen Reduction as a Route to Ammonia, ACS Sustain. Chem. Eng. 8 (2020) 8938–8948. doi:10.1021/acssuschemeng.0c01206.

[175] C.A. Fernandez, M.C. Hatzell, Editors' Choice—Economic Considerations for Low-Temperature Electrochemical Ammonia Production: Achieving Haber-Bosch Parity, J. Electrochem. Soc. 167 (2020) 143504. doi:10.1149/1945-7111/abc35b.